



# Major changes in diatom abundance, productivity, and net community metabolism in a windier and dryer coastal climate in the southern Humboldt Current

Bárbara G. Jacob<sup>d,\*</sup>, Fabián J. Tapia<sup>a,b,c</sup>, Renato A. Quiñones<sup>a,b</sup>, Rodrigo Montes<sup>a</sup>, Marcus Sobarzo<sup>a,b</sup>, Wolfgang Schneider<sup>b,e</sup>, Giovanni Daneri<sup>c,d</sup>, Carmen E. Morales<sup>b,e</sup>, Paulina Montero<sup>c,d</sup>, Humberto E. González<sup>f,g</sup>

<sup>a</sup> Centro Interdisciplinario para la Investigación Acuícola (INCAR), Universidad de Concepción, Chile

<sup>b</sup> Departamento de Oceanografía, Universidad de Concepción, Campus Concepción, Víctor Lamas 1290, Casilla 160-C, código postal: 4070043, Concepción, Chile

<sup>c</sup> Centro de Investigación Oceanográfica COPAS Sur-Austral, Universidad de Concepción, Concepción, Chile

<sup>d</sup> Centro de Investigación en Ecosistemas de la Patagonia (CIEP), Simpson 471, Coyhaique, Chile

<sup>e</sup> Instituto Milenio de Oceanografía (IMO), Universidad de Concepción, P.O. Box 1313, Concepción 3, Chile

<sup>f</sup> Universidad Austral de Chile, Instituto de Ciencias Marinas y Limnológicas, Casilla 567, Valdivia, Chile

<sup>g</sup> Centro FONDAP-IDEAL de Investigación en Ecosistemas Marinos de Altas Latitudes, Universidad Austral de Chile, Valdivia, Chile

## ARTICLE INFO

### Keywords:

Primary production  
Net metabolism  
Si:N ratio  
Upwelling-favorable winds  
River outflows  
South-central Chile

## ABSTRACT

Ongoing global warming caused by climate change has been suggested to produce an intensification of upwelling-favorable winds along the coast of south-central Chile due to a poleward displacement of the South Pacific Anticyclone (SPA). Here we explore the extent to which these changes have influenced water column properties, inorganic nutrients, primary production, diatom abundances and net community metabolism (GPP/CR) in these shelf waters. Our analysis is based on a monthly time series (2003–2013) of *in situ* oceanographic and biological observations and experiments to assess gross primary production (GPP) and community respiration (CR) at a shelf station in central Chile (~36.5°S), along with ancillary data on alongshore wind variability, river outflow and MODIS-derived surface fluorescence (nFLH). A reduction in river outflow from 2007 onwards, forced remotely by the poleward displacement of the SPA, resulted in a cooler and saltier water column, with lower dissolved Si:N ratios (Si(OH)<sub>4</sub>: NO<sub>3</sub><sup>-</sup>) and net community metabolism shifting from high net autotrophy (mean GPP/CR = 10.9 ± 14) to a balance between production and respiration (GPP/CR = 1.17 ± 0.6). A key finding was that most of the observed inter-annual variability in diatom abundance and primary production rates from 2003 to 2013 could be explained by two opposite trends: a significant intensification of upwelling-favorable winds during early spring (October–November) post-2009, and a sustained drop in freshwater discharged by the main local river during the same period. A combination of more intense equatorward winds and weaker stratification of the water column may have driven mixing and turbulence beyond the levels that are suitable for diatom growth when the upwelling period began (October–November), and subsequently may have enhanced the offshore transport of nutrients and productivity during late summer months (February–March). Patterns revealed by the analysis of monthly composites of normalized surface fluorescence (nFLH) are consistent with this interpretation. Further intensification of upwelling-favorable winds, combined with changes in the pattern of precipitation and river discharges, may have negative effects on the composition, productivity, and carbon export in shelf waters of this and other coastal upwelling ecosystems.

## 1. Introduction

Eastern boundary upwelling systems (EBUS) are among the most productive oceanic areas in the world (Chavez and Messié, 2009;

Quiñones et al., 2010), and strongly influence atmosphere-ocean CO<sub>2</sub> exchange as well as recycling of fixed carbon and its export to the open and deep ocean (Feely et al., 1999; Torres et al., 2003; Mathis et al., 2012). Consistent with the hypothesis that coastal upwelling is

\* Corresponding author.

E-mail address: [bjacob@udec.cl](mailto:bjacob@udec.cl) (B.G. Jacob).

<https://doi.org/10.1016/j.pocean.2018.10.001>

Received 12 January 2017; Received in revised form 1 October 2018; Accepted 2 October 2018

Available online 03 October 2018

0079-6611/ © 2018 Published by Elsevier Ltd.

intensified due to the warming pattern associated with climate change (Bakun, 1990; Bakun et al., 2010), long-term positive trends in upwelling-favorable wind intensity have been reported for the Peruvian coast (Bakun and Weeks, 2008), northwest Africa (Santos et al., 2005), South Africa (Shannon et al., 1992), California (Mendelsohn and Schwing, 2002; Snyder et al., 2003) and along the subtropical west coast of South America (Falvey and Garreaud, 2009). More recently, a meta-analysis of the literature on upwelling-favorable wind intensification in EBUS suggests that winds have intensified in the California, Benguela, and Humboldt upwelling systems and weakened in the Iberian system over timescales ranging up to 60 years (Sydeham et al., 2014).

Despite the ongoing increase in atmospheric greenhouse gases, the Earth's global average surface air temperature has remained more or less steady since 2001; a key component of this slowdown in surface warming is the strengthening of Pacific trade winds that account for the cooling of the tropical Pacific (England et al., 2014). Atmospheric modeling of western subtropical South America has predicted stronger equatorward alongshore winds on the Chilean coast due to intensification and poleward displacement of the South Pacific Anticyclone (SPA) under a climate warming scenario (Falvey and Garreaud, 2009; Belmadani et al., 2014). A recent time series analysis of *in situ* temperature and salinity observations over the continental shelf off south-central Chile between 2002 and 2013 (Schneider et al., 2017) showed an abrupt change in hydrographic conditions from 2007 onwards. This change was driven by a poleward displacement of the SPA that in turn has accelerated alongshore, upwelling-favorable winds, particularly during winter, injecting deeper colder water into the upper water column. The poleward displacement of the SPA since 2007 was also associated with substantial reductions in precipitation and river discharge in the southern Humboldt Current System (Schneider et al., 2017). The combination of these changes in atmospheric forcing resulted in a transition from warmer/fresher to cooler/saltier conditions in the nearshore water column, especially during winter months.

How climate warming might impact upon various EBUS systems has become a crucial question, because upwelling favorable equatorward wind scan have significant effects on water temperature (McGregor et al., 2008; Falvey and Garreaud, 2009), chemical parameters (Weeks et al., 2004), oxygen availability (Grantham et al., 2004; Hernández-Miranda et al., 2010; 2012) and biological components of the ecosystem (Iles et al., 2011; Escribano et al., 2012). High primary production rates ( $\sim 26 \text{ gC m}^{-2} \text{ d}^{-1}$ ) have been observed in the Humboldt Current System (HCS) in association with episodic upwelling-favorable events at around  $\sim 36^\circ\text{S}$  (Daneri et al., 2000; Montero et al., 2007), whereas winds causing persistent upwelling at around  $\sim 30^\circ\text{S}$  have consistently resulted in lower production rates (Montecino et al., 1996; Daneri et al., 2000).

In the region off south-central Chile ( $35\text{--}39^\circ\text{S}$ ), wind variability spans from diurnal (sea breeze) to synoptic (3–15 days) and seasonal periodicity (Sobarzo et al., 2007). The seasonal variability is modulated by latitudinal displacements of the SPA (i.e. equatorward in fall-winter and poleward in spring-summer), which promote the dominance of northerly downwelling-favorable winds in fall-winter and southerly upwelling-favorable winds in spring-summer (Sobarzo et al., 2007). Seasonally, water column stratification in this region is driven not only by wind but also by changes in the mixed-layer heat balance induced by solar radiation and by freshwater balance, which is dominated by austral winter maxima in river discharge and precipitation (Sobarzo et al., 2007). On the synoptic scale, periods of intense and persistent equatorward winds drive the upwelling of Equatorial Subsurface Water (ESSW), characterized by low oxygen and high concentrations of dissolved nutrients (Strub et al., 1998; Quiñones et al., 2010). These events alternate with calms, or reversals in wind that can last from 2 to 8 days (Daneri et al., 2012).

The coastal upwelling zone off south-central Chile is among the most productive areas within the HCS, with a strong seasonal signal in

total phytoplankton biomass and primary production induced by enhanced upwelling and solar radiation during the spring-summer months (Daneri et al., 2000; Montero et al., 2007; Anabalón et al., 2016). Phytoplankton biomass in this area tends to be concentrated in near-surface waters ( $< 20 \text{ m}$  depth), with maxima observed during spring-summer dominated by only a few diatom genera (Anabalón et al., 2007; González et al., 2007; Sanchez et al., 2012). The seasonality of nano-phytoplankton is lower, though with highest mean abundance and biomass also recorded during the upwelling season (Anabalón et al., 2007; Böttjer and Morales, 2007). The contribution of pico-phytoplankton to total chlorophyll-a (Chl-a) appears to be limited throughout the year in the area (Collado-Fabbri et al., 2011).

A decrease in the relative contribution of total pico-phytoplankton biomass has been observed between 2002 and 2012 in the southern coastal HCS ( $35\text{--}38^\circ\text{S}$ ), with an apparent trend of negative Chl-a anomalies during the upwelling season combined with positive (upwelling-favorable) wind anomalies (Corredor-Acosta et al., 2015). A negative trend in meso-zooplankton biomass was also reported during the same period (Escribano et al., 2012), together with a significant shifts in taxonomic and size composition from 2007 onwards (Medellin-Mora et al., 2016). Anabalón et al. (2016) observed that the micro-phytoplankton decreased in abundance and biomass during the upwelling seasons of 2006–2009 compared to 2002–2006, principally as a result of lower abundance of the diatoms *Skeletonema* and *Leptocylindrus*. The reduction in diatom abundance appeared to be associated with higher surface salinities and lower temperatures, but also with variations in Si:N and N:P ratios that could be related to changes in continental processes (Anabalón et al., 2016). High silicic acid (Si(OH)<sub>4</sub>) concentrations ( $50 \mu\text{M}$ ) in the lower reaches and in surface river plume waters of the nearby Biobío River during winter have been reported in the coastal area of Concepción ( $36^\circ\text{S}$ ) (Léniz et al., 2012) and may be an important silicate reservoir for diatom growth during spring-summer months in this coastal area (Sanchez et al., 2012). The presence of silicic acid is required in seawater to support diatom growth (Sarmiento et al., 2007), with the typical uptake ratio of silicic acid to dissolved inorganic nitrogen for diatom growth being ca. 1:1 (Brzezinski, 1985; Ragueneau et al., 2000). A decrease in the availability of silicic acid relative to nitrate can result in the predominance of other algal groups that require lower concentrations of silicic acid (Conley et al., 1993; Dortch et al., 2001; Dongyan et al., 2013).

In this study we assess the extent to which inter-annual changes in atmospheric forcing and hydrological conditions off south-central Chile have influenced water column properties over the continental shelf. Changes in water column properties can in turn impact upon physiological rates, net community metabolism and diatom abundance and composition in this highly productive coastal upwelling area. Our analyses are based on a monthly time series of *in situ* oceanographic and biological observations on the continental shelf off south-central Chile ( $36.5^\circ\text{S}$ ) that span 11 years (2003–2013). We contextualize these observations using ancillary data on wind stress variability and river outflow, together with ocean color data derived from satellite imagery.

## 2. Methods

### 2.1. Field sampling

In August 2002, the Center for Oceanographic Research in the eastern South Pacific (COPAS) initiated a monthly time series of hydrographic and biogeochemical observations at a station located  $\sim 20 \text{ km}$  offshore on the shelf off south-central Chile (St. 18,  $36^\circ 30.80'\text{S}$ – $73^\circ 07.75'\text{W}$ , depth 90 m; Fig. 1), between the submarine canyons of the Biobío River ( $36^\circ 52'\text{S}$ ) and the Itata River ( $36^\circ 05'\text{S}$ ). All cruises were carried out on board the R/V Kay-Kay of the Universidad de Concepción. During the 11-year period spanned by this study (Jan., 2003 – Dec., 2013), 110 surveys were conducted for CTD profiles during a total of 132 months (a monthly service was envisaged but

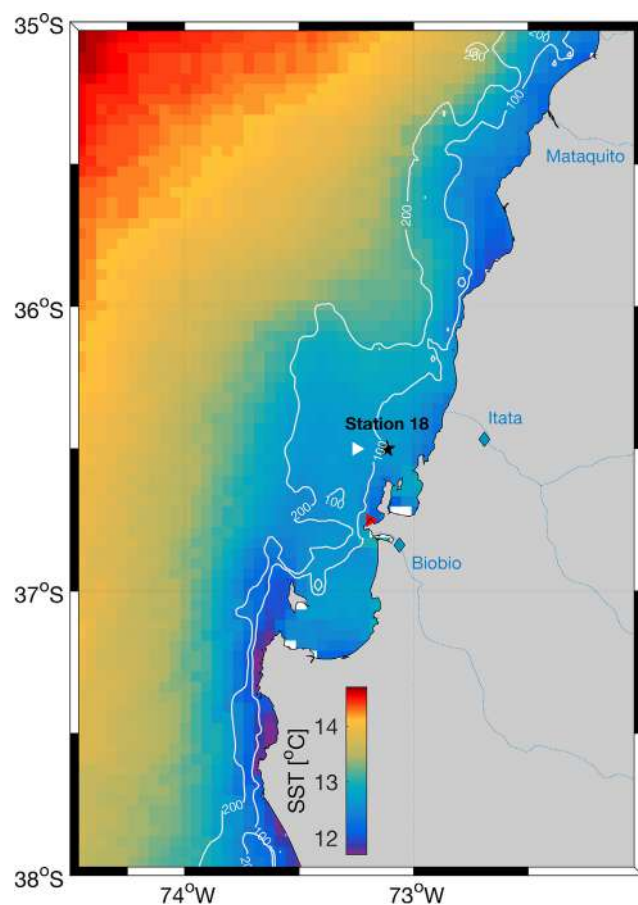


**Fig. 1.** Geographic location of the fixed time-series station (St. 18) over the south-central Chile continental shelf, superimposed on the average field of Sea Surface Temperature for the period 2003–2013. SST derived from Level 3 MODIS-Aqua imagery provided by the Ocean Biology Processing Group (OBPG) at NASA's Goddard Space Flight Center; white contours correspond to the 200 and 100 m isobaths. Triangles to the west and south of St. 18 indicate the geographic location for which Blended Seawinds (white) and weather station data at Pt. Hualpen (red) were obtained. Major rivers are shown in blue. Blue diamonds on the Itata and Biobio Rivers show the location of the hydrological stations for which daily outflow data were obtained. (For interpretation of the references to colour in this figure legend, the reader is referred to the web version of this article.)

coverage of ca. 83% was achieved). During the other months, the station could not be visited because of either bad weather or vessel maintenance. Of the total of 110 surveys, 108, 110 and 104 monthly measurements were carried out for dissolved nitrate, phosphate and silicic acid, respectively. The CTD was also equipped with an oxygen sensor, which was calibrated using a semi-automatic version of the Winkler method (Williams and Jenkinson, 1982; Knap et al., 1993). During several sampling dates (14 out of 110 cases) the oxygen sensor did not function and *in situ* oxygen titrations conducted during those cruises were used instead.

The lower boundary of the euphotic zone was determined as the depth at which PAR (photosynthetically active radiation) was 1% of the observed surface value. Discrete water samples for determinations of dissolved oxygen and inorganic nutrients ( $\text{NO}_3^-$ ,  $\text{PO}_4^{3-}$ ,  $\text{Si(OH)}_4$ ) were collected with Niskin bottles at depths of 0, 5, 10, 15, 20, 30, 40, 50, and 80 m. Samples for estimates of diatom abundance were obtained at depths of 0, 10 and 30 m (during 91, 118 and 63 monthly surveys, respectively). During 81 of the monthly surveys, additional water was collected to carry out incubations for primary production and community respiration.

## 2.2. Oceanographic data and dissolved nutrients

With up to six CTD casts conducted on any given cruise, average profiles of temperature and salinity could be constructed for each monthly visit to Station 18. Hydrographic profiles were displayed between 0 and 40 m depth to obtain better resolution of the variability in the upper water column. Missing data within the time series were filled using the climatological (2003–2013) monthly means adjusted for the temperature/salinity anomalies of the previous and following month (Schneider et al., 2017). For example: the highest seasonal surface temperatures occurred in February. When a February cruise was missed during an anomalously warm year, the missing data was replaced using the climatological mean for February plus the positive anomalies observed in January and March of that same year. Monthly anomalies of temperature and salinity were computed as the difference between the observed value and its climatological (2003–2013) mean value for the same month and depth (Supplementary material Fig. 1S).

Supplementary data associated with this article can be found, in the online version, at <https://doi.org/10.1016/j.pocean.2018.10.001>.

Samples for nitrate and phosphate were filtered (GF/F filters) on board while samples for silicic acid were not filtered. Subsequently, samples were frozen ( $-20^\circ\text{C}$ ) prior to analysis in the laboratory. Nutrients were determined using an auto-analyzer (Alpkem flow solution IV; period 2003–2009; Strickland and Parsons, 1972) and colorimetric methods (SEAL Analytical autoanalyzer; period 2010–2013; Grasshoff et al., 1983). The analytical error for the nutrient measurements was assessed through the coefficient of variation (CV) of the triplicate measurements for any given depth. Samples with a CV > 10% were not included in the nutrient database following the criterion of Farías et al. (2015). The detection limits for nitrate was  $0.75 \mu\text{mol L}^{-1}$ , for silicic acid  $0.67 \mu\text{mol L}^{-1}$  and  $0.051 \mu\text{mol L}^{-1}$  for phosphate.

## 2.3. Phytoplankton abundance

Samples for diatom counts (250 ml) were taken from the Niskin Bottle and preserved in buffered formalin (4%). Sub-samples of 20–50 ml were placed in settling chambers for 30 h prior to analysis under an inverted microscope (Zeiss Axiovert 200) using the standard methodology (Utermöhl, 1958). Diatoms were counted and identified at magnifications of 200–400x and were quantified by either by observing the entire sedimentation chamber, or by observing a portion of the chamber when abundance was high (i.e. transects or half the chamber). Taxa were identified with reference to taxonomic keys and relevant supporting literature (Rivera, 1969; Tomas, 1997). Diatoms quantified in the settling chambers included all micro-phytoplankton (> 20  $\mu\text{m}$ ) and most of the nano-phytoplankton fraction (2–20  $\mu\text{m}$ ). Although the magnification used (200–400 x) only allows reliable identification of diatoms larger than  $\sim 5 \mu\text{m}$  in size, abundance of small diatoms (< 5  $\mu\text{m}$ ) was never the dominant size group during the study period. Nevertheless, some chain-forming diatom genera such as *Skeletonema* and *Leptocylindrus* ( $\sim 5 \mu\text{m}$  in width) were accurately identified under the microscope. Analytical biases due to changes in personnel were minimized by using the same technician and microscope for the entire study. At least 100 cells of the most representative diatom species were counted using the Utermöhl method, and the uncertainty associated with these counts was around 10% error (Venrick, 1978). Finally, species diversity within the diatom assemblage was quantified with the Shannon-Weaver index  $H'$  (Shannon and Weaver, 1949):

$$H' = - \sum_{i=1}^S p_i \log_2 p_i \quad (1)$$

where  $p_i$  is the relative importance of species  $i$ , derived from cell numbers ( $N_i/N_t$ ).  $N_i$  is the number of cells of species  $i$  while  $N_t$  is the total number of cells for all recorded species.

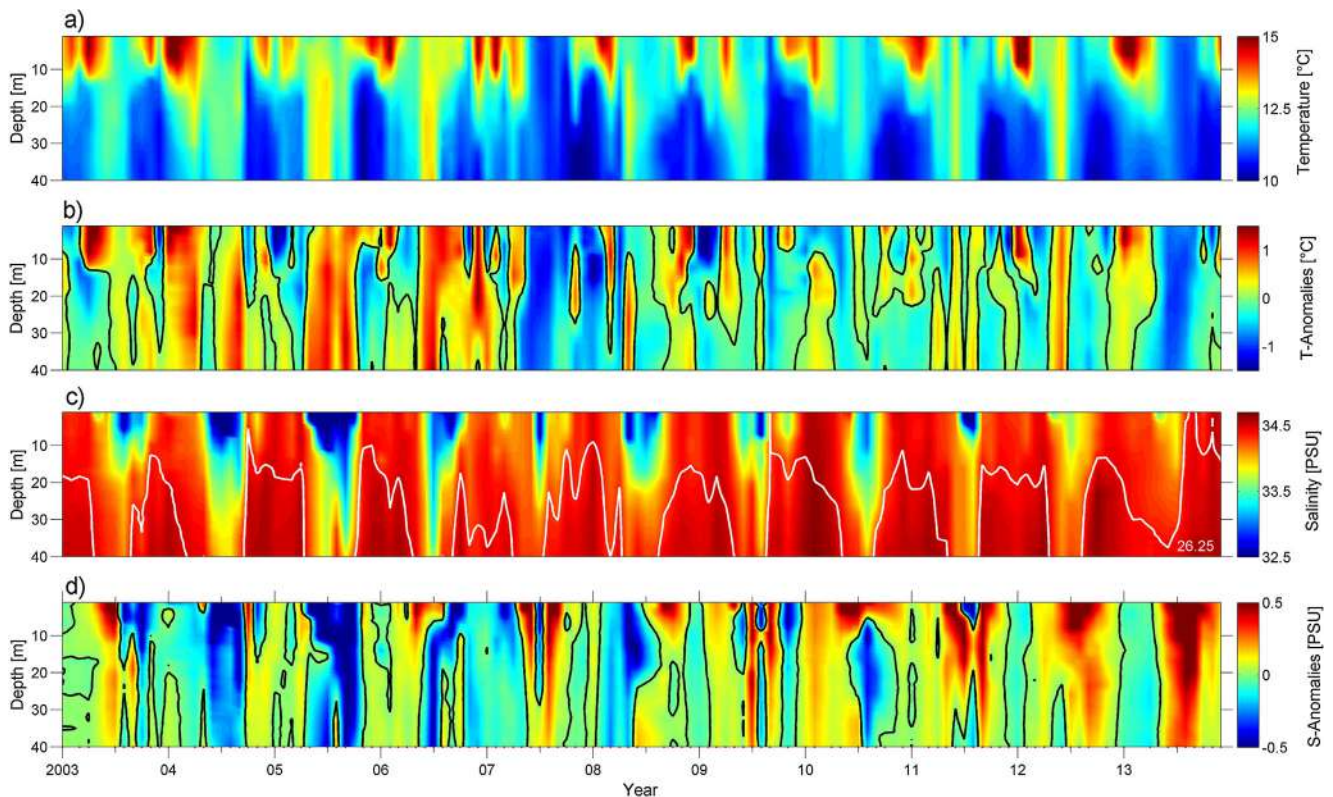


Fig. 2. St. 18 time series data (January 2003 – December 2013) for the upper layer (0–40 m depth): (a) Temperature. (b) Temperature anomalies (the zero anomaly contour is overlaid in black). (c) Salinity (a density contour  $\sigma_t = 26.25$  is overlaid in white indicating upwelling water). (d) Salinity anomalies (the zero anomaly contour is overlaid in black). Red dots on the bottom axis of the lower panel indicate months when St.18 sampling was conducted (see Section 2.2 on interpolation of data due to gaps).

#### 2.4. Gross primary production and community respiration experiments

Eighty-one experiments were carried out from September 2003 to October 2013 to estimate gross primary production (GPP) and community respiration (CR) at four depths within the euphotic zone: 2, 10, 20, and 30 m. Rates of GPP and CR were estimated from changes in dissolved oxygen concentration during incubations of light and dark bottles (Strickland, 1960). Water from Niskin bottles was transferred to gravimetrically calibrated 125-mL borosilicate bottles using a silicone tube; five time-zero bottles, five light bottles and five dark bottles were used for each incubation. Light and dark bottles were incubated at *in situ* light and temperature for  $9.7 \pm 1.5$  h using a surface-tethered mooring system; time-zero bottles were fixed at the beginning of each experiment. Dissolved oxygen concentration was measured using a semi-automatic version of the Winkler method (Williams and Jenkinson, 1982; Knap et al., 1993) based on an end-point photometric detector, a Dosimat 665 (Metrohm) titrator and a chart recorder. The uncertainty of these measurements was quantified as the coefficient of variation (CV) of the quintupled measurements conducted at time zero, and for light and dark bottles. The CV for all measurements was 1.32% (range: 0.028–12.49%), and samples with a CV > 10% were removed from the GPP and CR database. GPP values were converted from oxygen to carbon units using a conservative photosynthetic quotient (PQ) of 1.25, and to carbon CR values using a respiration quotient (RQ) of 1 (Laws, 1991). Rates of GPP and CR were calculated as follows:  $GPP = \text{mean } [O_2]_{\text{light}} - \text{mean } [O_2]_{\text{dark}}$  bottles;  $CR = \text{mean initial } [O_2] - \text{mean } [O_2]_{\text{dark}}$  bottles. Depth-specific GPP and CR rates were integrated using a polynomial method and were expressed in  $g\ C\ m^{-2}\ d^{-1}$ .

The GPP/CR ratio was used to determine net ecosystem metabolism of the microbial community (Smith and Hollibaugh, 1997). Where the GPP/CR ratio is > 1 the ecosystem is considered to be net autotrophic,

while ratios of < 1 indicate net heterotrophy. The system was deemed as in metabolic balance or “coupled” when most of the photosynthetic organic matter production was consumed within a 24-hour cycle ( $GPP/CR \sim 1$ ). The term “decoupled” was used when GPP and CR were out of phase for more than 24 h, so that the GPP/CR ratio was either > 1 or < 1.

#### 2.5. Time series of river outflow and its variability

To examine inter-annual variability in freshwater discharges into the area around Station 18, data on daily outflow for the two largest rivers in the region (Biobío and Itata) in 2000–2015 were obtained from the CR2 Center’s data platform (<http://explorador.cr2.cl>). Because the Itata data set had fewer gaps than the Biobío record (4% vs. 8% of 5,569 days), and taking into account the Itata river being closest and most likely to influence hydrographic conditions at Station 18, the analysis of trends in freshwater discharge at different times of the seasonal cycle was conducted only for this river. To test for trends or sudden changes in freshwater discharge, the daily outflow record available for the Itata river was time-integrated over 3-month periods corresponding to winter (June–August) and spring (September–November) of each year. Winter integrated outflow was compared to yearly changes in the latitudinal position of the South Pacific Anticyclone (SPA) during winter. Data on the position of the SPA were obtained from Schneider et al. (2017) and converted to anomalies by subtracting the long-term mean ( $-28.8403^\circ S$ ; computed over the period 1979–2013). Finally, the existence of a sudden change or a decreasing trend in springtime freshwater discharge over the study period were respectively tested with the non-parametric Pettitt test (Pettitt, 1979) for change-point detection and the Mann-Kendall trend test implemented in the R package “trend”v1.0.1.

(<https://www.rdocumentation.org/packages/trend>).

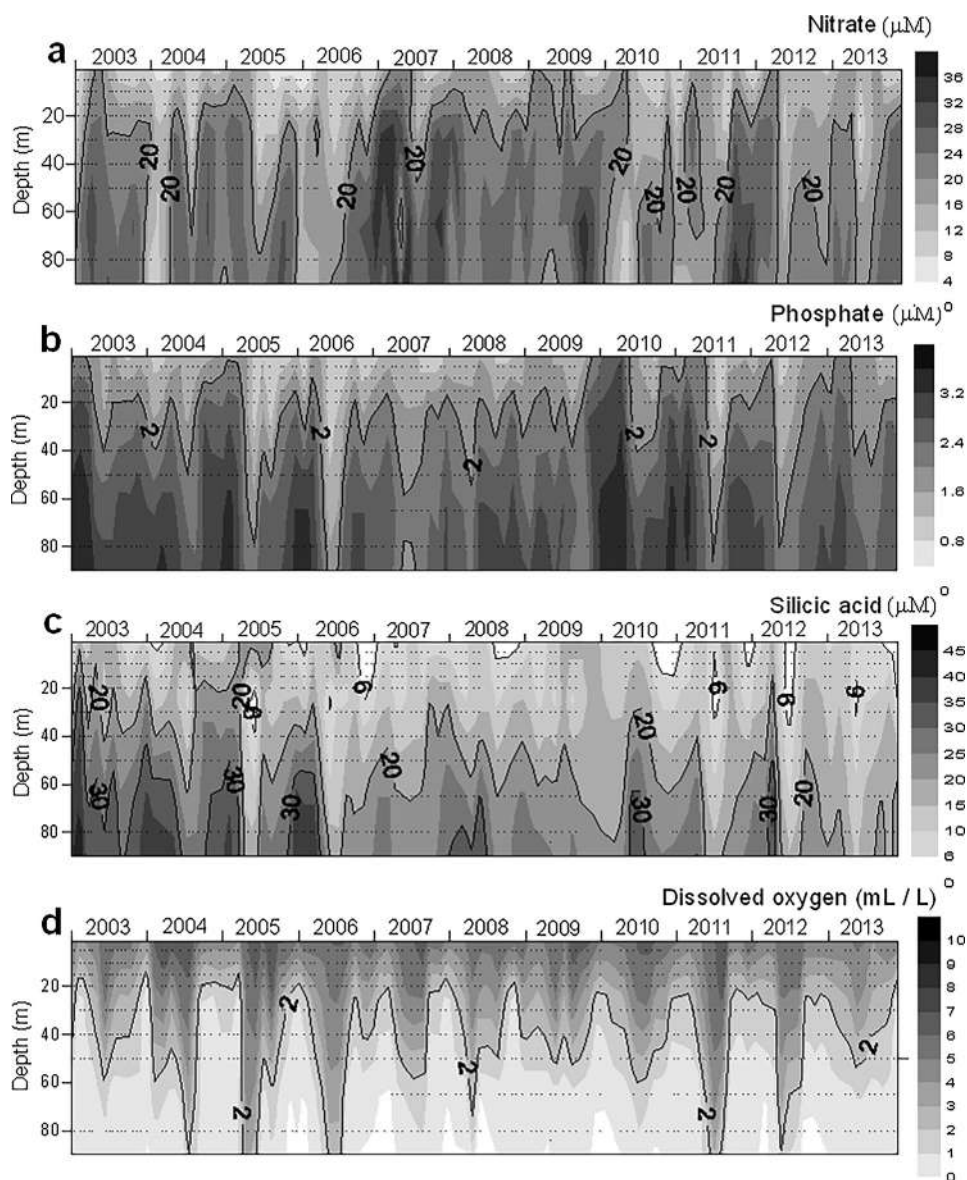


Fig. 3. St. 18 time series of dissolved inorganic nutrients and oxygen (January 2003 – December 2013): (a) Nitrate; (b) Phosphate; (c) Silicate; (d) Dissolved oxygen. Black dots in each panel represent the monthly sampling dates and the sampling depth.

## 2.6. Time series and climatology of wind stress

Data to characterize coastal wind variability in the area were obtained from two sources: a weather station located ca. 30 km south of Station 18 at Pt. Hualpen (see Fig. 1) and the Blended Sea Winds product provided by the NOAA National Center for Environmental Information ([www.ncei.noaa.gov](http://www.ncei.noaa.gov)), with spatial and temporal resolution of  $0.25^\circ$  and 1 day, respectively. Available wind measurements from the Hualpen station spanned only 4 years of the period studied here (2005–2009), and were also available from 2014 onwards. These two sets of *in situ* wind data were used as a reference to validate the use of Blended Seawinds over the entire study period.

Daily fields of surface wind velocity for a region delimited by  $35\text{--}40^\circ\text{S}$  and  $72\text{--}76^\circ\text{W}$  were downloaded from <https://www.ncei.noaa.gov/thredds/catalog/uv/daily> for a period spanning January 2000 through March 2017. From this grid of daily wind fields, a daily time series of wind velocity was extracted for a cell with coordinates  $36.5^\circ\text{S}$  and  $73.25^\circ\text{W}$  (i.e. 12 km west of St. 18). As indicated above, the correspondence between alongshore velocities from Seawinds and those measured at the shoreline of Hualpen was checked for two different

periods spanning 4 years (June 2005 – June 2009) and 3.2 years (Jan., 2014 – Mar., 2017). For each dataset, the alongshore component of wind velocity was obtained by rotating the wind vectors to align them with the main axis of variability identified in each case. The main axis of wind variability for Seawinds was almost aligned with geographic north ( $0.8^\circ\text{E}$ ), whereas wind at Pt. Hualpen had a main axis of variability that was roughly aligned with the shoreline and that ranged between  $21^\circ\text{E}$  for 2005–2009 and  $16^\circ\text{E}$  for 2014–2017. Least-squares regression was used to fit a linear model between Seawinds-derived and Hualpen alongshore velocities for each period. A good correspondence was observed between these daily records, both in terms of timing and magnitude of alongshore winds (see Supplementary Material Fig. 5S). Linear regression fits yielded models with  $r^2 = 0.65$  for 2005–2009 and  $r^2 = 0.68$  for 2014–2017. Although poleward velocities from Seawinds appeared to overestimate the *in situ* measurements, upwelling-favorable winds corresponded well with those measured *in situ*.

A daily time series of alongshore wind stress was obtained from the Seawinds record and used to analyze inter-annual variability of upwelling-favorable winds using three approaches. Firstly, we produced monthly climatologies for periods before (April 2000 – March 2010)

and after (April 2010 – March 2017) the observed drop in diatom abundance detected at Station 18 after the spring-summer season of 2009–2010 (see Fig. 4). The daily time series was used to analyze the frequency and duration of upwelling events during each spring-summer season, defined here as 1 October through 31 March of the following year. Within each season, upwelling events were identified as periods when alongshore wind stress exceeded and remained over a threshold of  $0.05 \text{ N m}^{-2}$  (see García-Reyes et al., 2014). The number of events thus identified and their duration (in days) were recorded for each season, and these data later analyzed for inter-annual trends. Finally, because of the differences in alongshore winds stress during the first third of the spring-summer season observed between the pre- and post-2010 climatologies, and considering the importance of that period for the subsequent diatom bloom, we quantified the alongshore stress accumulated during October and November of each year and tested whether (and when) a significant change had occurred using the non-parametric Pettitt test for change-point detection (see above).

## 2.7. Statistical analyses on biological and chemical databases

A Student's *t*-test was used to compare oceanographic data obtained during spring-summer and autumn-winter seasons. The Shapiro-Wilk statistic (Shapiro and Wilk, 1965) was used to check for normality, and the Levene test to check the homoscedasticity. When data were not normally distributed or showed heteroscedasticity, a non-parametric Mann-Whitney test was used to test for differences. To verify if the observation frequency affected the detection of a declining trend in diatom abundance over the 2003–2012 period, the following simulation analysis was conducted. First, missing observations from the monthly time series were filled by linear interpolation using adjacent values. For every year from 2003 to 2012 (a 10-year period) a random sampling of *S* monthly observations was conducted in order to construct *R* = 1000 re-sampled time series. We began randomly selecting *S* = 12 observations per year (which is equivalent to the total number of observations available in our study) and finished selecting *S* = 6 observations per year, which amounts to a reduction of 50% in available observations. For every re-sampled time series (*R*), a linear regression model was fitted using least squares. The statistical power *P*, i.e. the probability of successfully rejecting the null hypothesis when it is false (Bolker, 2008) was calculated for each iteration. In other words, we estimated the probability of detecting an effect, which in our case corresponded to a declining trend over time (Johnson et al., 2015). The statistical power of detecting a trend as a function of sample size was calculated for *R* = 1,000 re-sampled time series as:

$$P = \frac{\sum_{i=1}^R p < 0.05}{R} \quad (2)$$

Year 2013 was not considered in the analysis, given the number of missing observations for that year. Finally, Pettitt tests (Pettitt, 1979) were used to detect single change-points in the time series of inorganic nutrient ratios (Si:N and N:P) and Shannon-Weaver diversity indices. All missing data were filled with values from linear interpolation before applying the test. Nutrient ratios were calculated as bi-monthly averages between September 2003 and December 2008, thus producing two time series of *N* = 32 observations each. The Pettitt test was not applied after December 2008 due to the presence of missing data gaps of > 3 months in the nutrient time series. The same test was applied to the Shannon-Weaver monthly time series between January 2005 and December 2012 at 0 m depth (*N* = 96), and between January 2003 and December 2012 at 10 m depth (*N* = 120). Under the null hypothesis ( $H_0$ : no change point is detected), the non-parametric statistic  $K_T$  was estimated using the R software (R Development Core Team 2005, version 3.0.2) and the R package “trend” (Pohlert, 2016).

## 3. Results

### 3.1. Time series of hydrographic conditions

Temperature and salinity displayed a pronounced seasonal cycle (Fig. 2), with the water column influenced by solar radiation in the upper 15 m in late spring and summer. The seasonal temperature cycle at depths > 15 m was modulated by the upwelling of colder waters driven by southerly alongshore winds during the austral spring-summer. The 26.25 isopycnal (white contour in Fig. 2c) indicated that upwelled water during spring-summer months corresponded to Equatorial Subsurface Water (ESSW), according to Sobarzo et al. (2007).

Haline stratification was confined to autumn-winter months, fueled by the seasonal increase in precipitation and river discharge (Fig. 2c), as previously reported for this area (Sobarzo et al., 2007; Schneider et al., 2017). The influence of freshwater was most pronounced in the upper 15 m during 2003–2006 but weakened from 2007 onwards, and was almost undetectable during the winters of 2012 and 2013. At the inter-annual scale, average temperature and salinity anomalies in the upper 30 m (Fig. 2b, d and Supplementary Material Fig. 1S) exhibited two distinct hydrographic regimes: (i) a slightly warmer (temperature anomaly +0.18 °C) and fresher (salinity anomaly –0.13) regime observed between Jan., 2003 – Apr., 2007, and (ii) a slightly cooler (temperature anomaly –0.2 °C) and saltier (salinity anomaly +0.086) regime observed between May 2007 – August 2013.

### 3.2. Temporal variability of dissolved nutrients and oxygen

Depth-averaged nitrate and phosphate concentrations within the upper layer (0–30 m depth) were similar during the non-upwelling season (April–September) (15.43 μM; 1.57 μM, respectively) and the upwelling season (October–March) (15.81 μM; 1.85 μM, respectively). However, the variability (coefficient of variation; CV) was lower in the non-upwelling (phosphate: 19%; nitrate: 29%) compared to the upwelling season (phosphate: 55%; nitrate: 30%). Depth-averaged silicic acid was higher and less variable during the non-upwelling season (13.7 μM; CV = 35.6%) compared to the upwelling season (9.66 μM; CV = 80.1%). Nitrate concentrations of < 12 μM were often observed in the upper 15 m during the spring-summer season, suggesting consumption by biological activity (Fig. 3a), whereas contours for 20 μM nitrate and 2 μM phosphate at depths < 30 m (Fig. 3a and b) were suggestive of a renewal of nutrients within the euphotic zone.

At the inter-annual scale, the time series of silicic acid concentrations showed a decreasing trend in both the upper and lower layers (Fig. 3c). The 20 μM silicic acid contour ascended to depths < 30 m during 2003, 2004 and 2005, but remained deeper from the spring of 2006 onwards. Moreover, periods with low silicic acid concentrations (6 μM) within the top 15 m were increasingly observed since 2006. The seasonal distribution of dissolved oxygen in the water column (0–80 m) showed an ascent of the 2 ml L<sup>-1</sup> contour to depths < 30 m only during the spring-summer upwelling season (Fig. 3d). These low concentrations of dissolved oxygen together with the observed temperature-salinity characteristics during spring-summer are indicative the upwelling of Equatorial Subsurface Water (ESSW).

### 3.3. Diatom assemblages, plankton community rates and nutrient ratios

A total of 77 diatom species were identified during the study. Diatom assemblages showed strong seasonality in total abundance at both 0 m (*U* = 244; *n* = 60; *p* = 0.002) and 10 m depths (*U* = 151; *n* = 55; *p* = 0.001), and were mostly dominated by species of *Chaetoceros* (30.01%), *Skeletonema* (16.21%), *Thalassiosira* (10.41%) and *Leptocylindrus* (7.58%). Other species accounted for 35.5% of total diatom assemblages found during the upwelling season (Fig. 4). Mean diatom abundance at 10 m depth reached the highest values during summer 2003, spring-summer 2003/2004, spring-summer 2004/2005

and spring-summer 2005/2006 (mean:  $1.56 \times 10^6$  cell  $L^{-1}$ ; range:  $2.8 \times 10^3$ – $5.8 \times 10^6$  cell  $L^{-1}$ ), whereas lower diatom abundance was observed during the spring-summer seasons of 2006/2007 and 2007/2008 (mean:  $0.56 \times 10^6$  cell  $L^{-1}$ ; range:  $0$ – $1.5 \times 10^6$  cell  $L^{-1}$ ). Differences between these two periods, however, were not statistically significant ( $U = 136$ ;  $n = 39$ ;  $p > 0.05$ ). During spring-summer 2008/2009, diatom abundance increased to a mean of  $1.97 \times 10^6$  cell  $L^{-1}$  (range:  $1.06 \times 10^6$ – $3.6 \times 10^6$  cell  $L^{-1}$ ). Finally, diatom abundance decreased sharply from May 2009 until December 2013 ( $0.21 \times 10^6$  cell  $L^{-1}$ ; range:  $1.7 \times 10^3$ – $0.7 \times 10^6$  cell  $L^{-1}$ ) (Fig. 4). A similar pattern of variability in diatom presence was observed at 0 m depth, although cell abundances during spring-summer 2007/2008 were higher than at 10 m. Despite some missing data from depths of 0 and 30 m, inter-annual changes in diatom abundance were consistent with those observed for 10 m depth, and exhibited a similar drop from the spring-summer of 2010 onwards (except for one sample from 0 m in Jan., 2010). All samples collected from 2010 until the end of our study, and throughout the euphotic zone (0, 10, and 30 m depth), showed total diatom abundances below 1 million cells per liter.

Diatom abundance exhibited a declining trend during the entire period studied, although the simulation conducted to verify whether a change in observation frequency had influenced this trend indicated that a reduction in the number of monthly observations per year ( $S$ ) produced a drop in statistical power  $P$  (see Table 1). However, only a slight decrease of  $P$  was found for a reduction from  $S = 12$  to  $S = 8$  monthly observations within a year. A greater reduction in  $P$  (ca. 30%) occurred when  $S = 6$ . Since 80% power is typically considered adequate (Johnson et al., 2015), we concluded that having at least 7 observations per year ( $S = 7$ ) provided enough statistical power ( $P = 84.3$ , Table 1) to detect a declining trend. Our findings therefore indicated that the long term decrease of diatom abundance over time is robust, and does not represent an artifact resulting from limited number of available data points.

This decreasing trend of total diatom abundance was accompanied by a decrease in species diversity (Shannon-Weaver index,  $H'$ ). The application of Pettitt tests to detect single change-points in the Shannon-Weaver time series showed similar results for 0 and 10 m depth (Supplementary Material Fig. 2S). In both cases a significant change in diversity occurred after December 2008, as evidenced by the  $K_T$  statistic of the Pettitt test of 832 ( $p < 0.05$ ) for 0 m and 1571 ( $p < 0.01$ ) for 10 m depth. The mean Shannon index at 0 m dropped from 1.88 in 2003–2008 to 1.33 after December 2008, with a concurrent drop from 2.14 to 1.45 at 10 m depth (Supplementary Material Fig. 2S).

Time series measurements of GPP and CR at St. 18 (Fig. 5a, b) showed a marked seasonal cycle, with significantly different rates in the spring-summer and fall-winter seasons ( $U = 614$  and  $884$ ,  $n = 102$ ,  $p < 0.05$ , respectively). Depth-integrated GPP was highest (range:  $0.4$ – $25.8$   $gC\ m^{-2}\ d^{-1}$ ) between September and March, and lowest (range:  $0.1$ – $11.5$   $gC\ m^{-2}\ d^{-1}$ ) between April and August, with maximum levels recorded in December 2003 ( $25.8$   $gC\ m^{-2}\ d^{-1}$ ), January 2005 ( $17.6$   $gC\ m^{-2}\ d^{-1}$ ), and November 2006 ( $17.5$   $gC\ m^{-2}\ d^{-1}$ ). Spring-summer GPP rates showed a decreasing trend from September 2003 to October 2013. CR rates were also highest between September and March (range:  $0.07$ – $30.2$   $gC\ m^{-2}\ d^{-1}$ ), and lowest between April and August (range:  $0.01$ – $6.28$   $gC\ m^{-2}\ d^{-1}$ ). These CR rates peaked in December 2003 ( $30.2$   $gC\ m^{-2}\ d^{-1}$ ), October 2008 ( $11.8$   $gC\ m^{-2}\ d^{-1}$ ), and October 2010 ( $13.6$   $gC\ m^{-2}\ d^{-1}$ ). A seasonal cycle in GPP/CR ratios

was not detected (Fig. 5c), but the values showed high inter-annual variability with the highest decoupling (mean GPP/CR:  $10.9 \pm 14$ ; range:  $0.1$ – $51.8$ ) occurring between October 2004 and January 2007 when the GPP rates were  $> 3$   $gC\ m^{-2}\ d^{-1}$  with the exception of one value (GPP/CR = 20) measured in June 2006 ( $0.2$   $gC\ m^{-2}\ d^{-1}$ ). The lowest ratios (mean GPP/CR:  $1.17 \pm 0.6$ ; range:  $0.1$ – $3.06$ ) occurred from February 2007–October 2013. Differences in GPP/CR ratios between pre- and post 2007 were significant ( $U = 381$ ;  $n = 74$ ,  $p = 0.003$ ).

Dissolved nutrient ratios (raw data) from January 2003–December 2013 showed a clear decrease in Si:N during 2006 and an increase of N:P during 2005 (Supplementary Material Fig. 3S). The Pettitt test showed a significant breakpoint in the N:P ratio ( $K_T = 191$ ,  $p < 0.01$ ) after September–October 2005, whereas the Si:N ratio dropped significantly ( $K_T = 274$ ,  $p = 0.0001$ ) after July–August 2006 (Supplementary Material Fig. 4S). The N:P ratio increased from 8.74 to 11.37 and the Si:N decreased from 1.04 to 0.50 in periods before and after the change point.

#### 3.4. Inter-annual flow of the Biobío and Itata rivers and its relationship to salinity and Si:N ratio

An inter-annual trend of decreasing freshwater discharges during the past decade is apparent from the time series, for both major rivers in the area (Fig. 6a). Changes in the freshwater outflow from the Itata River integrated over winter months (June through August) were positively correlated ( $r = 0.75$ ,  $p = 0.001$ ) with changes in the wintertime latitudinal position of the South Pacific Anticyclone (Fig. 6b). In addition, mean outflows of the Biobío and Itata Rivers in autumn–winter (May–September) were negatively correlated with the average salinity in the upper layer (0–30 m) ( $r = 0.63$ ;  $n = 55$ ;  $p < 0.0001$  and  $r = 0.66$ ;  $n = 55$ ;  $p < 0.0001$ , respectively) (Fig. 7a, b). The linear relationship observed between average salinity (0–30 m) and Si:N ratio (0–30 m) during the winter season ( $r^2 = 0.59$ ;  $n = 25$ ;  $p < 0.0001$ ) indicated that most of the variance in Si:N ratios can be explained by changes in salinity (Fig. 7c). We found no direct relationship between Si:N ratios and river discharges.

#### 3.5. Time series of wind stress measurements

The daily time series of alongshore wind stress (Fig. 8a) exhibited the seasonal pattern in upwelling/downwelling conditions that has been previously reported for this region. Upwelling-favorable winds are predominant during spring-summer months, and episodic strong poleward winds occur during the winter. Inter-annual variability appeared to manifest itself in two ways: an apparent increase in the frequency of wind fluctuations during the summer after 2010–2011, and a weakening of poleward winds during winter months after 2011 (Fig. 8a). This observation was supported by the wind climatologies computed for alongshore wind stress, which showed that until 2010 the monthly means exhibited the expected seasonal reversal, with poleward winds occurring in May–August and equatorward winds from September through April of the following year (Fig. 8b). After 2009, however, mean alongshore wind stress remained positive through most of the winter, barely crossing the zero line in August. An apparent intensification of springtime wind stress was also apparent, with stronger upwelling-favorable winds in October and November, prior to the months during which diatoms typically bloom (Fig. 8b).

The duration of events with upwelling-favorable winds exhibited an asymmetrical distribution in all seasons, with median durations (and upper quartiles) that ranged between 2 and 4 d (and 4–6 d) (Fig. 8c). Three seasons (2006, 2013, 2014) were exceptions to this pattern and exhibited longer events, with median durations (and upper quartiles) of 5–6 d (and 7–9 d). Consistent with the longer duration of events during these seasons the total number of events recorded between October and March dropped from ca. 25 to less than 20.

**Table 1**

Statistical power ( $P$ ) calculated for  $S$  available observations per year using  $R = 1000$  resampled time series.

Number of observations per year ( $S$ )	12	11	10	9	8	7	6
Power ( $P$ , %)	100	100	99.7	98.1	93.3	84.3	72.7

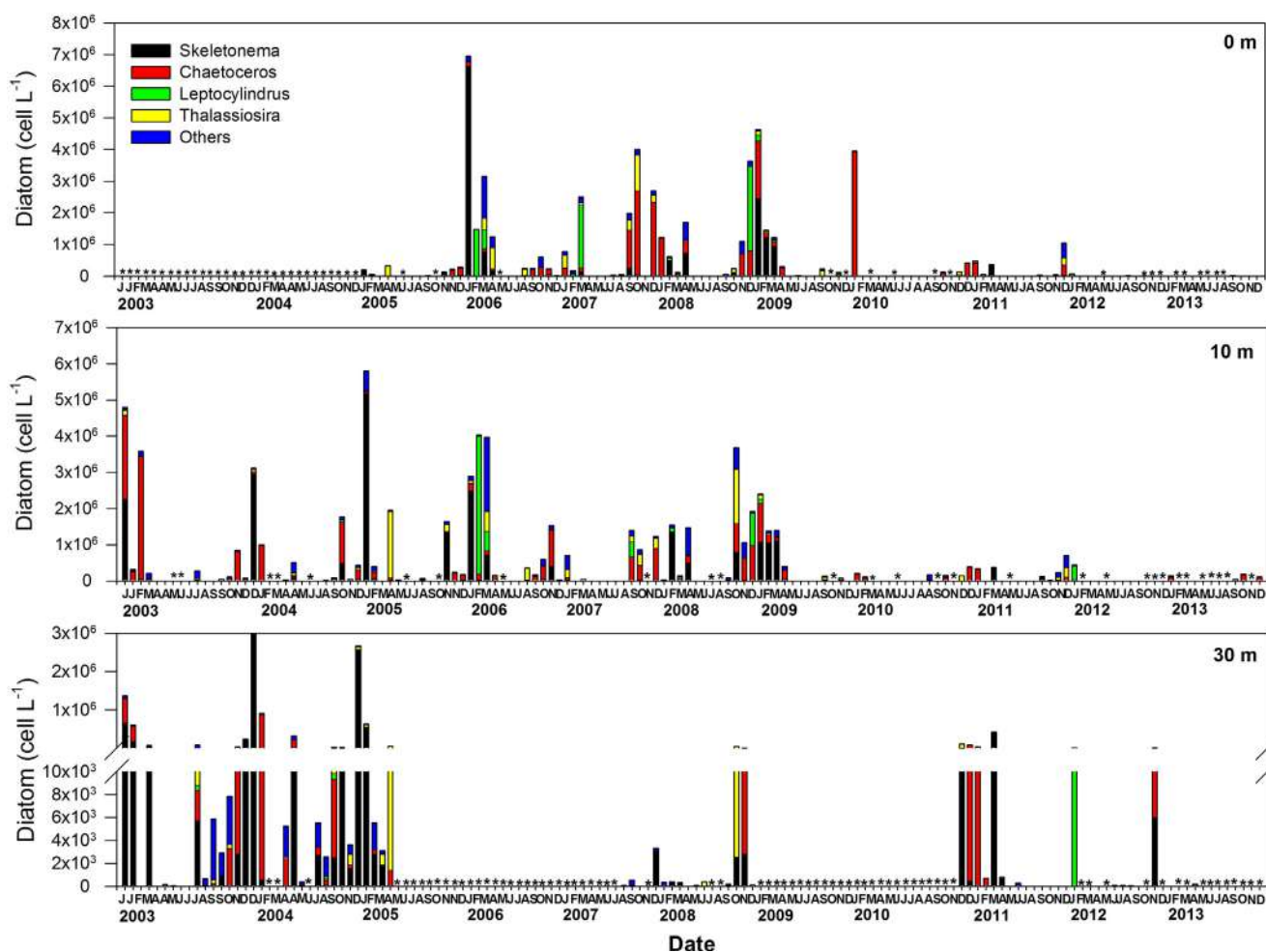


Fig. 4. Raw data of total diatom abundance and taxonomic composition obtained from St. 18 at 0, 10 and 30 m depth from January 2003 to December 2013. In some months two oceanographic samplings were conducted (e.g. 2003, 2004 and others). Asterisks indicate missing data, whilst months without asterisks and a bar indicate that diatom abundances ranged between 0 and  $4.7 \times 10^4$  cell  $L^{-1}$  (0 m depth),  $0-3 \times 10^4$  cell  $L^{-1}$  (10 m depth) and 0 and 80 cell  $L^{-1}$  (30 m depth).

During the first two months of spring (October–November), the inter-annual change in cumulative alongshore stress showed a clear increase after 2009 (Fig. 8d). A Pettitt test applied to this time series indicated that the post-2009 increase in cumulative alongshore stress for October–November was statistically significant ( $K_T = 68$ ,  $p = 0.01$ ), whereas no change in cumulative stress was observed during December–January ( $K_T = 26$ ,  $p = 0.92$ ). Cumulative stress in February–March also showed a trend to increase after 2009; however, the change was not statistically significant ( $K_T = 46$ ,  $p = 0.17$ ). Concurrent with the post-2009 intensification of wind forcing during the first months of spring, there was an apparent decrease in the springtime discharge of freshwater from the Itata River relative to the years prior to 2009 (Fig. 8d). However, this trend was not statistically significant (Mann-Kendall test,  $p = 0.15$ ).

#### 4. Discussion

The upwelling-driven nitrate flux to the euphotic zone is usually identified as the main mechanism driving new primary production in Eastern Boundary Upwelling Systems (Messié et al., 2009; García-Reyes et al., 2014). Changes in this supply of upwelled nitrate have often been invoked to explain ecosystem changes at scales ranging from seasonal (e.g., Barth et al., 2007) to multi-decadal (Roemmich and McGowan, 1995; Chavez et al., 2003; Rykaczewski and Checkley, 2008). Here we have shown that alongshore wind alone is not sufficient to understand fluctuations in the biological component, and particularly the primary

production of this coastal upwelling ecosystem. Inter-annual changes in hydrological conditions and patterns of alongshore wind stress, both forced by changes in the latitudinal position of the SPA, appear to have jointly driven a temporal shift in the composition and productivity of coastal phytoplankton, as well as in net community metabolism in these highly productive shelf waters off central Chile ( $36.5^\circ S$ ).

Inter-annual changes in net community metabolism (GPP/CR) were associated with the shift in hydrographic conditions from warmer/fresher to cooler/saltier, and a drop in silicic acid concentrations within the euphotic layer that drove Si:N ratios below 0.5 from August 2006 onwards. The timing of these shifts is consistent with the documented southward displacement of the SPA in 2007 (Schneider et al., 2017), and our data also demonstrate a positive correlation between the latitudinal position of the SPA and river discharge into the coastal ocean (Fig. 6). Negative anomalies (i.e., southward displacement) in the wintertime position of the SPA appeared associated with a reduction in river outflow and a subsequent increase in surface salinity at Station 18 (Schneider et al., 2017). Although we did not find a direct relationship between Si:N ratios and river discharges, most of the variance in Si:N ratios at Station 18 during autumn–winter can be explained by changes in surface salinity. Wintertime freshwater discharge may increase the supply of silicic acid from land to coastal waters thus increasing dissolved Si:N ratios in the study area. The observed reduction of silicic acid concentrations in the upper water column after July–August 2006, together with a dryer coastal climate and reduced river discharges since 2007, suggests that fluvial sources are the main drivers of changes in

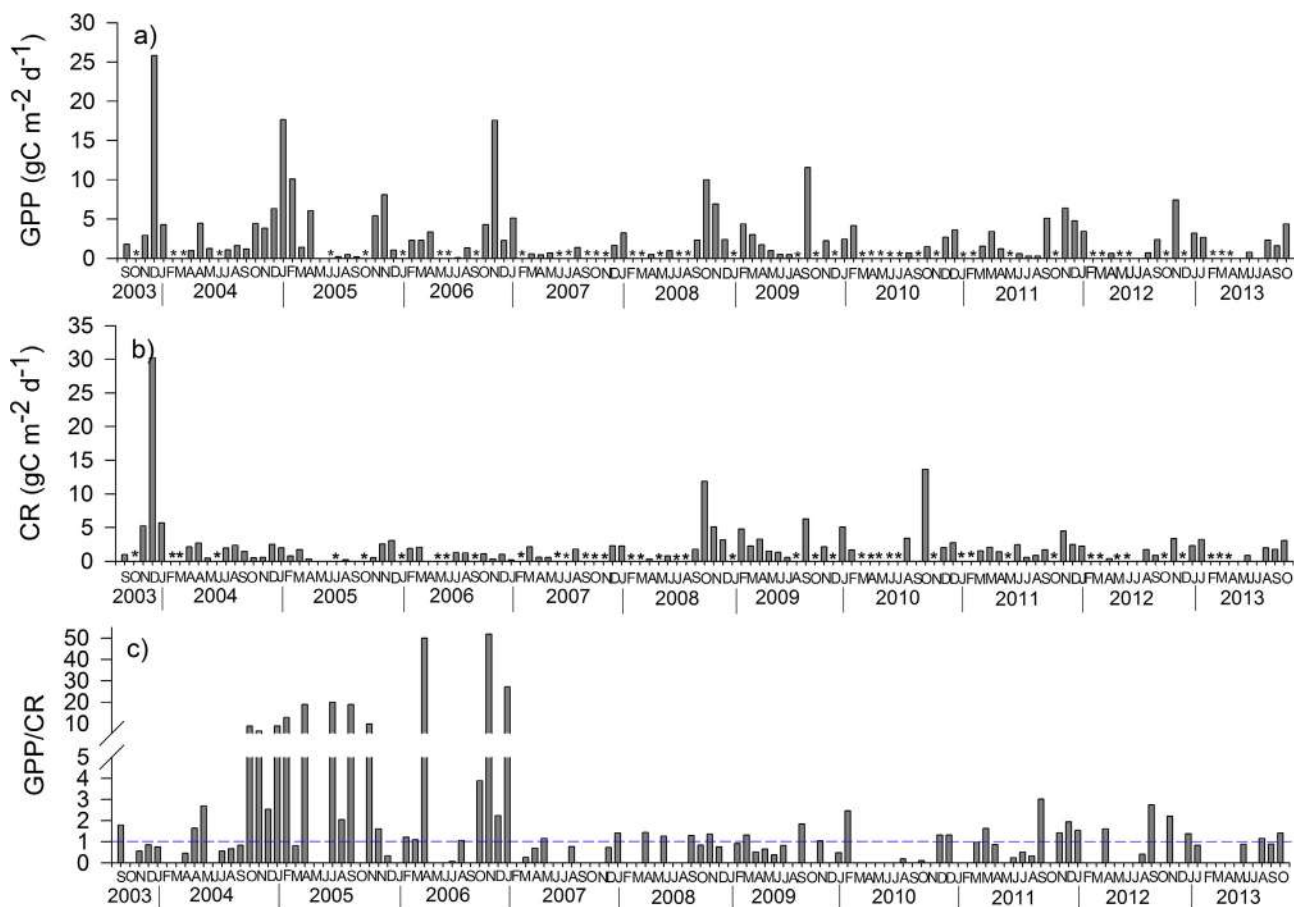


Fig. 5. Integrated monthly measurements obtained from St. 18 (September 2003 – October 2013) (0–30 m depth) on: (a) gross primary production (GPP), (b) community respiration (CR) and (c) community net metabolism (GPP/CR). Vertical lines below the x axis correspond to 1 January of each year. Dashed blue line indicates that GPP = CR. Asterisks indicate missing data for GPP, CR and GPP/CR, whilst months without asterisks and bar indicate GPP and CR rates <math>< 0.3 \text{ g C m}^{-2} \text{ d}^{-1}</math>.

dissolved Si. However, more studies will be required to elucidate the complex interplay between the oceanic Subantarctic Surface Water (SAASW), rich in dissolved inorganic nitrogen (DIN) but poor in dissolved silicic acid (Zentara and Kamykowski, 1981; Hutchins et al., 2001; Sarmiento et al., 2007), and river discharges that are rich in DSI in this area.

The mechanisms that underlie inter-annual fluctuations (i.e. net community metabolism shifting from high net autotrophy to near

balance between production and respiration) in this coastal ecosystem are not well understood. Studies conducted elsewhere have suggested that the size structure of autotrophs may be an essential factor for the GPP versus CR relationship in the plankton community (Legendre and Le Fèvre, 1995; Smith and Kemp, 2001; Teira et al., 2001, Jacob et al., 2011). Changes in GPP/CR ratios could also be driven by variations in the taxonomic composition of the phytoplankton resulting from variable physiological responses to silicic acid concentration within the

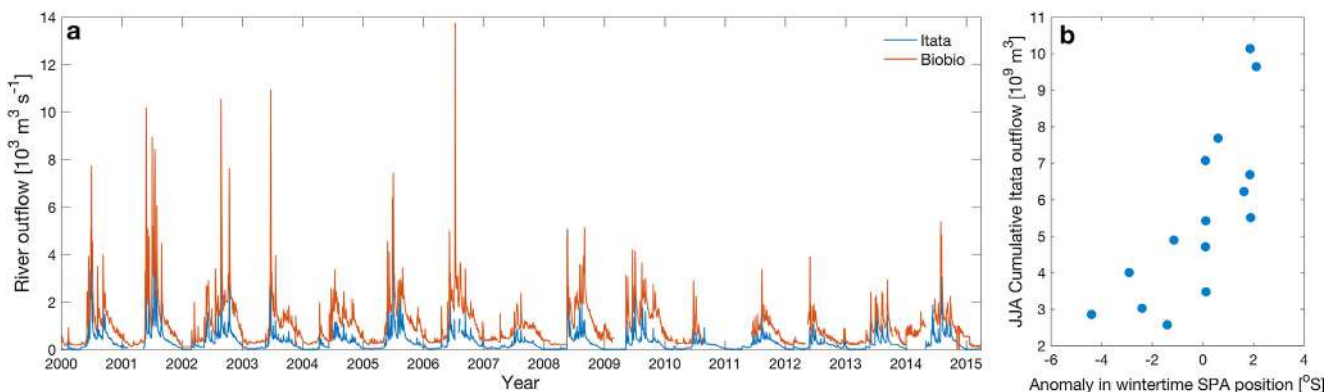
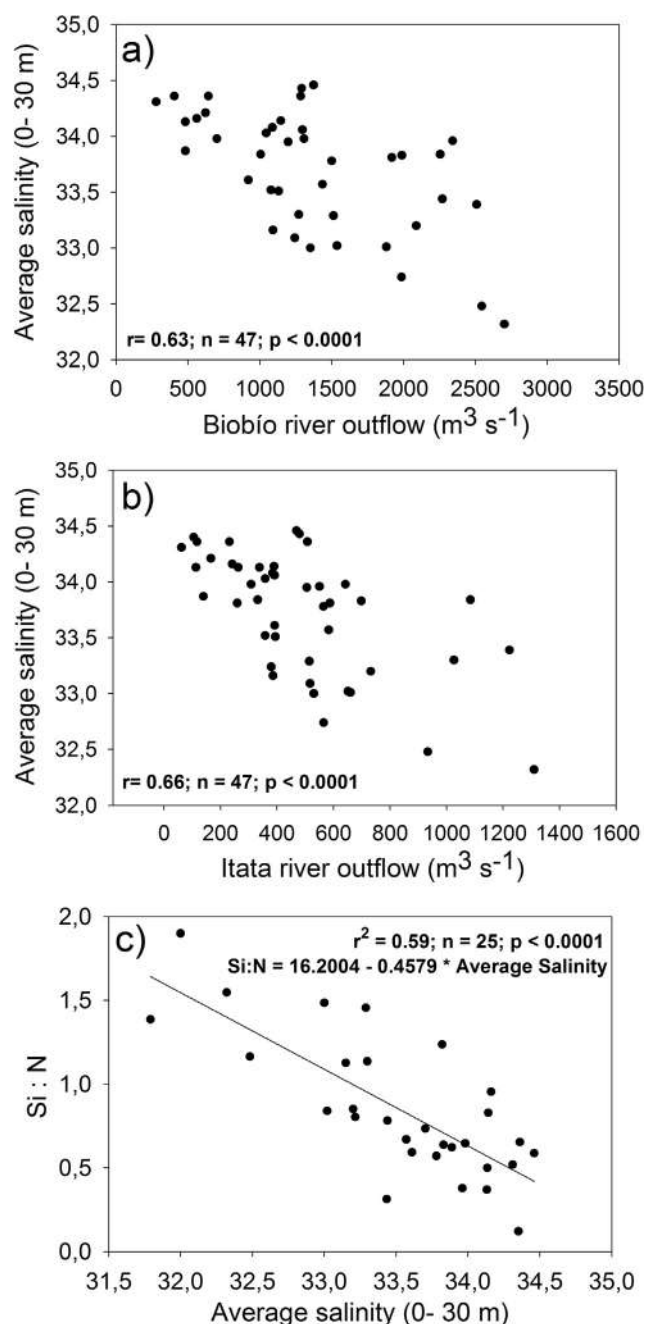


Fig. 6. (a) Daily outflow time series for the two main rivers discharging freshwater into the area around Station 18: Itata River (blue) and Biobio River (orange). Ticks on the x axis correspond to 1 January of each year. (b) Relationship between the winter (June through August) freshwater discharge of the Itata River and the winter anomaly in the latitudinal position of the South Pacific Anticyclone (SPA). Data on SPA position is taken from Schneider et al. (2017, Fig. 7c). (For interpretation of the references to colour in this figure legend, the reader is referred to the web version of this article.)



**Fig. 7.** (a) and (b) Pearson correlation between Biobío and Itata River outflows and average salinity (0–30 m) from St. 18 during winter (May–September 2003–2013). (c) Linear relationship between average salinity and Si:N ratio (average for 0–30 m depth in both cases) during autumn–winter seasons, based on *in situ* St. 18 data (2003–2013). Biobío and Itata River outflow data were obtained from the CR2 Centefs data platform (<http://explorador.cr2.cl>).

assemblage (Yamamoto and Tsuchiya, 1995; Nelson and Dortch, 1996). A comparison of diatom abundance at Station 18 between 2002 and 2006 and 2006–2009 showed a substantial reduction in the abundance of *Skeletonema* (ca. 82%) and *Leptocylindrus* (ca. 66%), with *Chaetoceros* and *Thalassiosira* remaining virtually unchanged in their abundance over the same period (Anabalón et al., 2016). Together, the diatom genera *Skeletonema*, *Chaetoceros* and *Thalassiosira* account for > 70% of total diatom abundance at Station 18, and play an important role in the transfer of organic material between the upper water column and shelf sediments during spring–summer (González et al., 2007).

The ratio of uptake of silicic acid to nitrogen during diatom growth

is typically ca. 1:1 (Brzezinski, 1985; Ragueneau et al., 2000), and a decrease in the availability of dissolved Si relative to nitrogen can cause a pronounced drop in the growth rate of diatoms and increased growth of non-siliceous phytoplankton taxa (Conley et al., 1993; Dortch et al., 2001; Dongyan et al., 2013). Although the minimum silicic acid concentrations detected in the upper layer (ca. 6  $\mu\text{M}$ ) may not be low enough to limit diatom growth rates (e.g. < 2  $\mu\text{M}$ ) (see Egge and Aksnes, 1992), lower concentrations of silicic acid could have occurred without detection within our monthly sampling interval. Moreover, diatoms may be uptake limited without being growth limited (Martin-Jézéquel et al., 2000 and cited therein), and at station 18, diatoms may have experienced kinetic limitation, especially when Si:N ratios were closer to 0.25 (Gilpin et al., 2004) during the period between 2007 and 2009 (average: 0.49; range: 0.2–0.9). Kinetic limitation could result in lower silicification rates (i.e. reduced silica per cell) to avoid growth limitation by suboptimal Si concentration, and this limitation could be species specific with consequent shifts in composition of phytoplankton assemblages. This could have potential indirect consequences for biogeochemical fate (e.g. less ballasted cells, reduced export efficiency, higher susceptibility to grazing, increased remineralization efficiency).

We do not have sediment trap data for the period 2003–2013, but published observations from sediment trap deployments at Station 18 in 2002–2005 did indeed indicate that higher sedimentation rates during the productive season tended to coincide with diatom dominance and elevated fluxes of particulate organic carbon (Montero et al., 2007; González et al., 2007). In fact, GPP rates and vertical fluxes of particulate organic carbon and Si are tightly coupled to the contribution of zooplankton pellets (González et al., 2007). Lower dissolved Si in the SPA-affected waters after 2007 could be coupled with reduced export efficiency driven by reduced Si/cell (caused by kinetic limitation), and a larger fraction of fixed carbon potentially respired in the surface layer. We therefore suggest that photosynthetically fixed carbon available for export to the deep ocean or to higher trophic levels may have been higher between 2003 and 2006, than after 2007.

While community net metabolism exhibits relationships with atmospheric (SPA position), hydrological (river outflow) and chemical (silicic acid) conditions, a key finding of our study is that two opposite trends could explain most of the observed inter-annual variability in diatom abundance and primary production rates between 2009 and 2013. Firstly, the intensification of upwelling-favorable winds and secondly, a sustained drop in freshwater discharged by the main rivers during the spring months. Our analyses have confirmed that a decline in diatom abundance has indeed occurred throughout the euphotic zone at Station 18, with abundances below 1 million cells per liter recorded since the spring of 2010. This decline in diatom abundance was associated with significant changes in diatom diversity from 2009 onwards when upwelling-favorable winds in the spring months (October–November) intensified significantly.

The intensification of equatorward winds in the region, combined with a weakened stratification at Station 18 after 2007 (Schneider et al., 2017), resulted in stronger upwelling (Pino-Pinuer et al., 2014) and a deepening of the mixed layer during the 2008–2010 period (Station 18; Medellín-Mora et al., 2016). This may have driven higher levels of mixing and turbulence with consequences for light limitation of diatom growth. These changes may have driven the levels of mixing and turbulence beyond those suitable for diatom growth. Alternatively, or additionally, an increase in losses of phytoplankton biomass from the coastal band may have also occurred due to enhanced offshore advection of surface waters, which is consistent with a growing body of literature that suggests a non-monotonic relationship between alongshore wind and the biological response in EBUSs. These strong winds appear to negatively affect primary productivity and phytoplankton biomass through physical mechanisms, such as enhanced offshore advection (and loss) of coastal nutrients and organic matter, and subduction of phytoplankton below the euphotic zone through stronger mixing or turbulence. In the upwelling system off northern Africa, Huntsman and

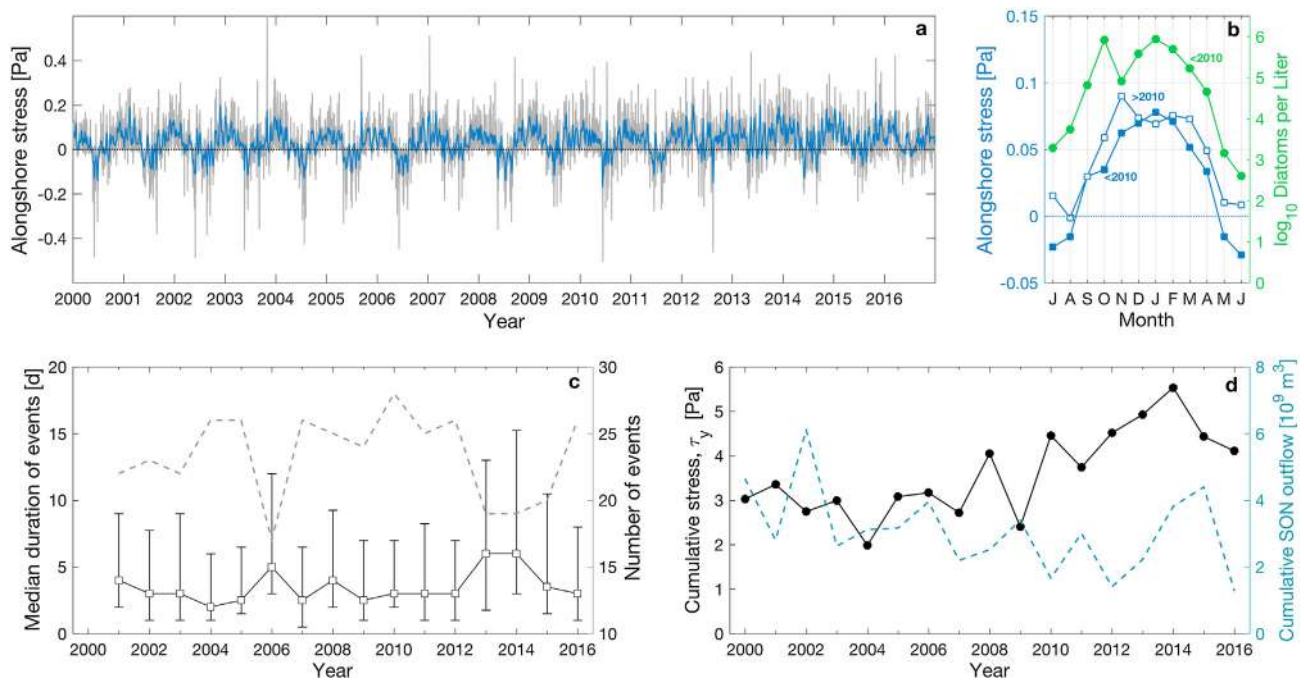


**Fig. 8.** (a) Time series of alongshore stress derived from Blended Seawinds for a cell centered at 36.5°S–73.25°W near St. 18 (see Fig. 1), with daily data and a 5-day running mean indicated by gray and blue lines, respectively; ticks on the x axis correspond to 1 January of each year. (b) Summer-centered monthly climatology of alongshore wind stress (blue) and diatom abundance (green) at St. 18. Wind climatology was computed for two different periods: April 2000 – March 2010 (filled symbols) and April 2010 – March 2017 (empty symbols), while the climatology of diatom abundance was computed using data collected until March 2010. (c) Median ( $\pm$  25% and 75% quartiles) of the duration of upwelling-favorable wind events (black line and symbols) together with the number of events (gray dashed line) detected for each spring-summer season (October–March). (d) Inter-annual variability of cumulative alongshore wind stress for October–November (black), together with fluctuations in cumulative outflow of the Itata River for September–November of each year (blue dashed line). (For interpretation of the references to colour in this figure legend, the reader is referred to the web version of this article.)

Barber (1977) found that photosynthesis was depressed during periods of deep mixing which maintained cells at depths where PAR light was 10% of surface levels. In the California Current System, elevated concentrations of chlorophyll-*a* have been found over 300 km offshore of the productive coastal upwelling region, demonstrating the importance of mesoscale physical dynamics in horizontal carbon transport (Barth et al., 2002; Plattner et al., 2005). Processes leading to the subduction, cross-shore transport, and downstream advection of upwelled water masses are frequent and persistent in the California Current System (Bograd and Mantyla, 2005; Messié and Chavez, 2015; Nagai et al., 2015). An idealized circulation model of coastal upwelling, coupled to an ecosystem model, showed that in the presence of mesoscale activity, the downward and offshore export of phytoplankton, zooplankton, and detritus significantly contributes to total export of organic matter out of the surface coastal ocean (Lathuilière et al., 2010). Additionally, in the four most productive EBUSs, relationships between satellite-derived estimates of net primary production, upwelling intensity, and eddy-kinetic energy suggested that high levels of eddy activity tend to result in low levels of biological production (Gruber et al., 2011). A summertime study conducted on the Oregon coast (Evans et al., 2015) proposed that rapid offshore advection and subsequent subduction of phytoplankton before it could exhibit a significant growth response, was a likely explanation for the persistently low chlorophyll levels and elevated pCO<sub>2</sub> observed in surface waters throughout an upwelling event.

In the HCS ( $\sim$ 36°S), high primary production rates ( $\sim$ 26 gC m<sup>-2</sup> d<sup>-1</sup>) have been associated with episodic upwelling-favorable events (Daneri et al., 2000; Montero et al., 2007), while areas with persistent upwelling winds at  $\sim$ 30°S have consistently exhibited lower production rates (Montecino et al., 1996; Daneri et al., 2000). Off Coquimbo (30°S), productivity rates are consistently in the lower range of primary production rates found in other upwelling centers within the HCS off Chile and Peru (Daneri et al., 2000). For example, depth integrated GPP

obtained off Coquimbo at the COSMOS station (coastal) during November 1997 was 2.8 gC m<sup>-2</sup> d<sup>-1</sup> (Daneri et al., 2000), a rate similar to those reported for coastal (0.1–2.9 gC m<sup>-2</sup> d<sup>-1</sup>) and oceanic (0.2–1.3 gC m<sup>-2</sup> d<sup>-1</sup>) areas by Montecino et al. (1996). This lower productivity has been attributed to strong upwelling (Daneri et al., 2000), although other processes, such as iron limitation, could also be considered (Torres and Ampuero, 2009). In the present study, GPP rates averaged 3.81 gC m<sup>-2</sup> d<sup>-1</sup> and ranged between 1.46 gC m<sup>-2</sup> d<sup>-1</sup> and 11.55 gC m<sup>-2</sup> d<sup>-1</sup> from 2009 onwards during the productive season when the upwelling favourable winds were intensified. This rate was comparatively higher than GPP at Coquimbo suggesting that at Station 18, the intensification of upwelling favourable winds since 2009/2010, did not reduce phytoplankton productivity compared to Coquimbo.

The relationship between turbulence and phytoplankton productivity may, therefore, need to be re-analyzed in the context of physical factors such as upwelling intensity under a climate-change scenario. Accordingly, the relationship between upwelling and productivity is thought to be dome-shaped (Bakun et al., 2015). When upwelling is weak, limited nutrient input restricts primary productivity, but when upwelling is too strong, turbulence could drive light limitation due to the deepening of the mixed layer, and planktonic organisms may be advected offshore. Moderate upwelling winds appear to result in optimal conditions for phytoplankton growth, and the occurrence of blooms that can support small-pelagic fisheries in EBUS (Cury and Roy, 1989). Such relationships between upwelling intensity and productivity have been documented in the nearshore environment within the California Current System (Jacox et al., 2016).

In the present study, the evaluation of mechanisms involved in the observed drop of diatom abundance was somewhat limited by having data from a single station on the continental shelf. Therefore, we have also used satellite information based on surface fluorescence as an appropriate proxy for distribution of phytoplankton biomass in the surface

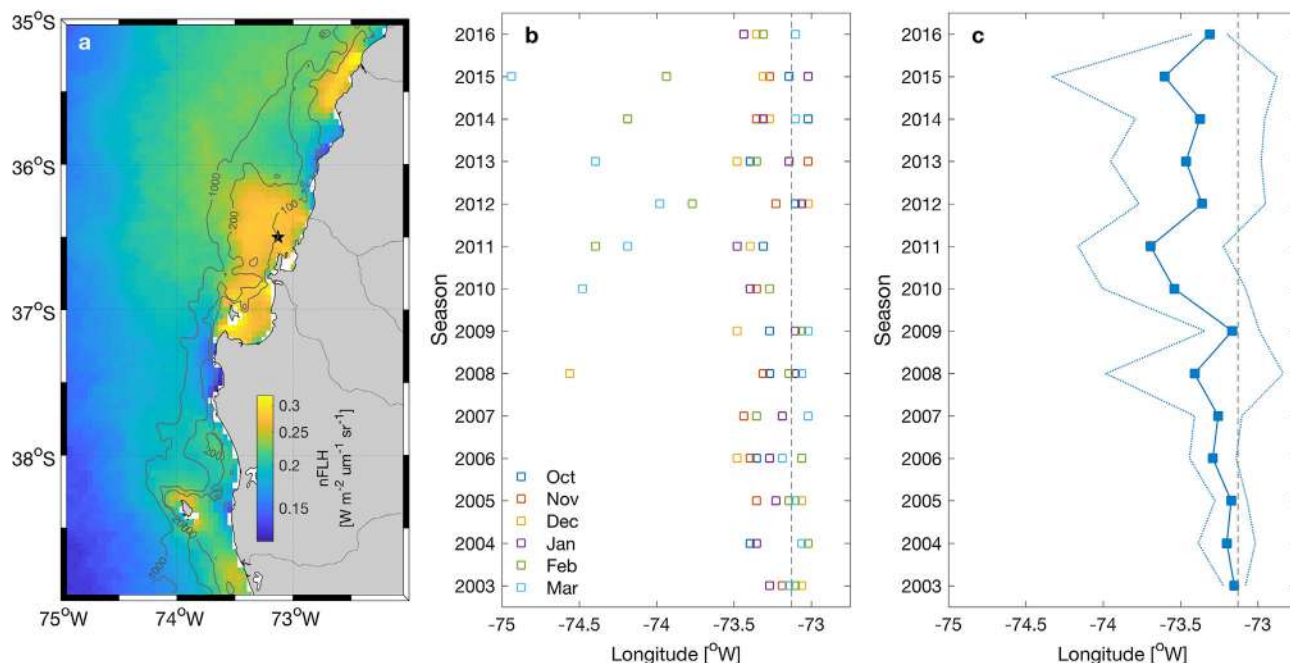


**Fig. 9.** (a) Long-term (2003–2017) mean field of normalized surface fluorescence (nFLH) derived from MODIS-Aqua monthly composites. (b) Inter-annual variability in the cross-shore position of the nFLH maximum at latitude 36.5 S (i.e. Station 18) for each monthly composite of spring-summer (October through March of the following year). (c) Mean ( $\pm 1$  SD) position of the nFLH maximum for each spring-summer month along the time series. The dashed vertical line in panels (b) and (c) corresponds to the cross-shelf position of Station 18.

layer (< 20 m depth). The bulk of the phytoplankton in this coastal zone is concentrated within this layer, and diatoms contribute largely to total fluorescence or Chl-a during the upwelling period (Anabalón et al., 2016). Data derived from monthly composites of MODIS-Aqua normalized fluorescence (nFLH) for this area of study (35–39°S, ca. 73–75°W; Fig. 9) indicated that, since 2010, there has been an offshore shift (ca. 100 km) in the cross-shore position of the fluorescence maximum (corresponding to Station 18), at least during the upwelling period of February and March. Accordingly, we found that higher diatom abundances and productivity rates prior to 2010 were associated with moderate wind stress values (cumulative wind stress: 2–4 Pa); whereas lower diatom abundances and productivity were associated with higher cumulative wind stress: > 4.5 Pa. Our observations on interannual changes in diatoms are consistent with other recent findings based on satellite time series of Chl-a and wind stress (2002–2012) for the coastal region between 35 and 38°S, which suggest a negative trend in Chl-a associated with upwelling intensification during the upwelling season, with lower Chl-a values observed after 2008 (Corredor-Acosta et al., 2015).

Our findings suggest that further intensification of upwelling-favorable winds (diatom growth being light-limited), combined with changes in the pattern of precipitation and river discharges (lower Si in the SPA-affected waters), may have adverse effects on the composition, productivity and carbon export in shelf waters of this and other coastal upwelling ecosystems. Given the current trends and predictions for future climate scenarios regarding coastal winds, precipitation and river discharges in eastern boundary currents, further work is needed to improve our understanding of the potential impacts of these factors on nearshore primary productivity, phytoplankton composition, and food webs in upwelling ecosystems.

## Acknowledgements

This research was funded by the Center for Oceanographic Research in the eastern South Pacific (FONDAP-COPAS Center, Research Grant No. 150100007), the Interdisciplinary Center for Aquaculture Research

(INCAR; FONDAP Grant No.15110027; CONICYT, Chile), and by COPAS Sur-Austral (CONICYT PIA PFB31). H. González was also partially funded by FONDAP-IDEAL 15150003. We thank all the personnel involved in the coastal time series of the COPAS Center and the captain and crew of the L/C Kay-Kay and L/C Kay-Kay II for their support throughout the sampling program.

## References

- Anabalón, V., Morales, C.E., Escribano, R., Varas, M.A., 2007. The contribution of nanoplanktonic assemblages in the surface layer (0–30 m) under different hydrographic conditions in the upwelling area off Concepción, central Chile. *Prog. Oceanogr.* 75, 396–414.
- Anabalón, V., Morales, C.E., Gonzalez, H.E., Menschel, E., Schneider, W., Hormazabal, S., Valencia, L., Escribano, R., 2016. Micro-phytoplankton community structure in the coastal upwelling zone off Concepción (central Chile): Annual and inter-annual fluctuations in a highly dynamic environment. *Prog. Oceanogr.* 149, 174–188.
- Bakun, A., 1990. Global climate change and intensification of coastal open upwelling. *Science* 247, 198–201.
- Bakun, A., Weeks, S.J., 2008. The marine ecosystem off Peru: what are the secrets of its fishery productivity and what might its future hold? *Prog. Oceanogr.* 79, 290–299.
- Bakun, A., Field, D.B., Redondo-Rodríguez, A., Weeks, S.J., 2010. Greenhouse gas, upwelling-favorable winds, and the future of coastal ocean upwelling ecosystems. *Global Change Biol.* 16, 1213–1228.
- Bakun, A., Black, B.A., Bograd, S.J., García-Reyes, M., Miller, A.J., Rykaczewski, R.R., Sydeman, W.J., 2015. Anticipated effects of climate change on coastal upwelling ecosystems. *Curr. Clim. Chang. Rep.* 1, 85–93.
- Barth, J.A., Cowles, T.J., Kosro, M.P., Shearman, K.R., Huyer, A., Smith, R.L., 2002. Injection of carbon from the shelf to offshore beneath the euphotic zone in the California Current. *J. Geophys. Res.* 107. <https://doi.org/10.1029/2001JC000956>.
- Barth, J.A., Menge, B.A., Lubchenko, J., Chan, F., Bane, J.M., Kirincich, A.R., McManus, M.A., Nielsen, K.L., Pierce, S.D., Washburn, L., 2007. Delayed upwelling alters nearshore coastal ocean ecosystems in the northern California current. *Proc. Nat. Acad. Sci.* 104, 3719–3724.
- Belmadani, A., Echevin, V., Codron, F., Takahashi, K., Junquas, C., 2014. What dynamics drive future wind scenarios for coastal upwelling off Peru and Chile? *Clim. Dyn.* <https://doi.org/10.1007/s00382-013-2015-2>.
- Böttjer, D., Morales, C.E., 2007. Nanoplanktonic assemblages in the upwelling area off Concepción (~36°S), central Chile: Abundance, biomass, and grazing potential during the annual cycle. *Prog. Oceanogr.* 75, 415–434.
- Bograd, S.J., Mantyla, A.W., 2005. On the subduction of upwelled waters in the California Current. *J. Mar. Res.* 63, 863–885.
- Brzezinski, M.A., 1985. The Si:C:N ratio of marine diatoms: interspecific variability and the effect of some environmental variables. *J. Phycol.* 21, 347–357.
- Bolker, B.M., 2008. *Ecological Models and Data* in R. Princeton University Press, 396 pp.

- Chavez, F.P., Ryan, J., Lluch-Cota, S.E., Niquen, M., 2003. From anchovies to sardines and back: multidecadal change in the Pacific Ocean. *Science* 299, 217–221.
- Chavez, F.P., Messié, M., 2009. A comparison of eastern boundary upwelling ecosystems. *Prog. Oceanogr.* 83, 80–96.
- Conley, D.J., Schelske, C.L., Stroemer, E.F., 1993. Modification of the biogeochemical cycle of silica with eutrophication. *Mar. Ecol. Prog. Ser.* 101, 179–192.
- Corredor-Acosta, J.A., Morales, C.E., Hormazabal, S., Andrade, I., Correa-Ramirez, M.A., 2015. Phytoplankton phenology in the coastal upwelling region off central-southern Chile (35°S–38°S): Time-space variability, coupling to environmental factors, and sources of uncertainty in the estimates. *J. Geophys. Res. Oceans*. <https://doi.org/10.1002/2014JC010330>.
- Collado-Fabbri, S., Vulot, D., Ulloa, O., 2011. Structure and seasonal dynamics of the eukaryotic picophytoplankton community in a wind-driven coastal upwelling ecosystem. *Limnol. Oceanogr.* 56, 2334–2346.
- Cury, P., Roy, C., 1989. Optimal environmental window and pelagic fish recruitment success in upwelling areas. *Can. J. Fish. Aquat. Sci.* 46, 670–680.
- Daneri, G., Dellarossa, V., Quiñones, R.A., Jacob, B., Montero, P., Ulloa, O., 2000. Primary production and community respiration in the Humboldt Current Systems off Chile and associated oceanic areas. *Mar. Ecol. Prog. Ser.* 197, 41–49.
- Daneri, G., Lizárraga, L., Montero, P., González, H.E., Tapia, F.J., 2012. Wind forcing and short-term variability of phytoplankton and heterotrophic bacterioplankton in the coastal zone of the Concepción upwelling ecosystem (central Chile). *Prog. Oceanogr.* 92, 92–96.
- Dongyan, L., Shen, X., Di, B., Shi, Y., Keesing, J.K., Wang, Y., Wang, Y., 2013. Palaeoecological analysis of phytoplankton regime shifts in response to coastal eutrophication. *Mar. Ecol. Prog. Series* 475, 1–14.
- Dortch, Q., Rabalais, N.N., Turner, R.E., Qureshi, N.A., 2001. Impacts of changing Si/N ratios and phytoplankton species composition. In: Rabalais, N.N., Turner, R.E. (Eds.), *Coastal hypoxia: consequences for living resources and ecosystems*. *Coast. Estuar. Stud. Ser.*, pp. 37–48.
- Edge, J.K., Aksnes, D.L., 1992. Silicate as regulating nutrient in phytoplankton competition. *Mar. Ecol. Prog. Series* 83, 281–289.
- England, M.H., McGregor, S., Spence, P., Meehl, G.A., Timmermann, A., Cai, W., Gupta, A.S., McPhaden, M.J., Purich, A., Santoso, A., 2014. Recent intensification of wind-driven circulation in the Pacific and the ongoing warming hiatus. *Nat. Clim. Chang.* 4, 222–227.
- Escribano, R., Hidalgo, P., Fuentes, M., Donoso, K., 2012. Zooplankton time series in the coastal zone off Chile: Variation in upwelling and responses of the copepod community. *Prog. Oceanogr.* 97, 174–186.
- Evans, W., Hales, B., Strutton, P.G., Shearman, R.K., Barth, J.A., 2015. Failure to bloom: Intense upwelling results in negligible phytoplankton response and prolonged CO<sub>2</sub> outgassing over the Oregon shelf. *J. Geophys. Res.* 120, 1446–1461.
- Falvey, M., Garreaud, R.D., 2009. Regional cooling in a warming world: Recent temperature trends in the southeast Pacific and along the west coast of subtropical South America (1979–2006). *J. Geophys. Res.* 114 (1–16), D04102. <https://doi.org/10.1029/2008JD010519>.
- Fariás, L., Besoain, V., García-Loyola, S., 2015. Presence of nitrous oxide hotspots in the coastal upwelling area off central Chile: an analysis of temporal variability based on ten years of a biogeochemical time series. *Environ. Res. Lett.* <https://doi.org/10.1088/1748-9326/10/4/044017>.
- Feely, R.A., Wanninkhof, R., Takahashi, T., Tans, P., 1999. Influence of El Niño on the equatorial Pacific contribution to atmospheric CO<sub>2</sub> accumulation. *Nature* 398, 597–601.
- García-Reyes, M., Largier, J.L., Sydeman, W.J., 2014. Synoptic-scale upwelling indices and predictions of phyto- and zooplankton populations. *Prog. Oceanogr.* 120, 177–188. <https://doi.org/10.1016/j.pocean.2013.08.004>.
- Gilpin, L.C., Davidson, K., Roberts, E., 2004. The influence of changes in nitrogen:silicon ratios on diatom growth dynamics. *J. Sea Res.* 51, 21–35.
- Grantham, B.A., Chan, F., Nielsen, K.J., Fox, D.S., Barth, J.A., Huyer, A., Lubchenko, J., Menge, B.A., 2004. Upwelling-driven nearshore hypoxia signals ecosystem and oceanographic changes in the northeast Pacific. *Nature* 429, 749–754.
- Grasshoff, K., Ehrhardt, M., Kremling, K., 1983. *Methods of Seawater Analysis*, second ed. Springer, Switzerland, pp. 419.
- González, H.E., Menshel, E., Aparicio, C., Barría, C., 2007. Spatial and temporal variability of microplankton and detritus, and their export to the shelf sediments in the upwelling area off Concepción, Chile (~36°S), during 2002–2005. *Prog. Oceanogr.* 75, 435–451.
- Gruber, N., Lachkar, Z., Frenzel, H., Marchesiello, P., Münnich, M., McWilliams, J.C., Nagai, T., Plattner, G.-K., 2011. Eddy-induced reduction of biological production in Eastern boundary upwelling systems. *Nat. Geosci.* 4, 787–792.
- Hernández-Miranda, E., Quiñones, R.A., Aedo, G., Valenzuela, A., Nermoud, N., Román, C., Yañez, F., 2010. A major fish stranding caused by a natural hypoxic event in a shallow bay of the eastern South Pacific Ocean. *J. Fish Biol.* 76, 1543–1564.
- Hernández-Miranda, E., Veas, R., Labra, F.A., Salamanca, M., Quiñones, R.A., 2012. Response of the epibenthic macrofaunal community to a strong upwelling-driven hypoxic event in a shallow bay of the southern Humboldt Current System. *Mar. Environ. Res.* 79, 16–28.
- Huntsman, S.A., Barber, R.T., 1977. Primary production off northwest Africa: the relationship to wind and nutrient conditions. *Deep-Sea Res.* 24, 25–33.
- Hutchins, D.A., Sedwick, P.N., DiTullio, G.R., Boyd, P.W., Quéguiner, B., Griffiths, F.B., Crossley, C., 2001. Control of phytoplankton growth by iron and silicic acid availability in the Subantarctic Southern Ocean: experimental results from the SAZ Project. *J. Geophys. Res.* 106, 2156–2202.
- Iles, A.C., Gouhier, T.C., Menge, B.A., Steward, J.S., Haupt, A.J., Lynch, M.C., 2011. Climate-driven trends and ecological implications of event-scale upwelling in the California Current System. *Global Change Biol.* <https://doi.org/10.1111/j.1365-2486.2011.02567>.
- Jacob, B., Daneri, G., Quiñones, R.A., Sobarzo, M., 2011. Community metabolism, phytoplankton size structure and heterotrophic prokaryote production in a highly productive upwelling zone off northern Chile. *Mar. Ecol. Prog. Ser.* 430, 23–34.
- Jacox, M.G., Hazen, E.L., Bograd, S.J., 2016. Optimal environmental conditions and anomalous ecosystem responses: Constraining bottom-up controls of phytoplankton biomass in the California Current System. *Sci. Rep.* 6, 12 pp. <https://doi.org/10.1038/srep27612>.
- Johnson, P.C.D., Barry, S.J.E., Ferguson, H.M., Müller, P., 2015. Power analysis for generalized linear mixed models in ecology and evolution. *Methods Ecol. Evol.* 6, 133–142.
- Knap, A.H., Michaels, A.F., Dow, R.L., Johnson, R.J., Gundersen, K., Sorensen, J.C., Clos, A.R., Howse, F.A., Hammer, M., Bates, N., Doyle, A., Waterhouse, T., 1993. *US Joint Global Flux Study, Bermuda Atlantic Time-series Study. BATS Methods Manual, Version 3*, Woods Hole, MA.
- Lathuilière, C., Echevin, V., Lévy, M., Madec, G., 2010. On the role of the mesoscale circulation on an idealized coastal upwelling ecosystem. *J. Geophys. Res.* 115. <https://doi.org/10.1029/2009JC005827>.
- Laws, E.A., 1991. Photosynthetic quotients, new production and net community production in the open ocean. *Deep-Sea Res.* 38, 143–167.
- Léniz, B., Vargas, C.A., Ahumada, R., 2012. Characterization and comparison of micro-phytoplankton biomass in the lower reaches of the Biobío river and the adjacent coastal area off central Chile during autumn-winter conditions. *Lat. Am. J. Aquat. Res.* 40, 847–857.
- Legendre, L., Le Fèvre, J., 1995. Microbial food webs and the export of biogenic carbon in oceans. *Aquat. Microb. Ecol.* 9, 69–77.
- Martin-Jézéquel, V., Hildebrand, M., Brzezinski, M.A., 2000. Silicon metabolism in diatoms: implications for growth. *J. Phycol.* 36, 821–840.
- Mathis, J.T., Pickart, R.S., Byrne, R.H., McNeil, C.L., Moore, G.W.K., Juranek, L.W., Liu, X., Ma, J., Easley, R.A., Elliot, M.M., Cross, J.N., Reisdorph, S.C., Bahr, F., Morison, J., Lichendorf, T., Feely, R.A., 2012. Storm-induced upwelling of high pCO<sub>2</sub> waters onto the continental shelf of the western Arctic Ocean and implications for carbonate mineral saturation states. *Geophys. Res. Lett.* 39, L07606.
- McGregor, H.V., Dima, M., Fischer, H.W., Mulitza, S., 2008. Rapid 20th-century increase in coastal upwelling off northwest Africa. *Science* 315, 637–639.
- Medellin-Mora, J., Escribano, R., Schneider, W., 2016. Community response of zooplankton to oceanographic changes (2002–2012) in the central/southern upwelling system of Chile. *Prog. Oceanogr.* 142, 17–29.
- Mendelsohn, R., Schwing, F.B., 2002. Common and uncommon trends in SST and wind stress in the California and Peru-Chile current systems. *Prog. Oceanogr.* 53, 141–162.
- Messié, M., Ledesma, J., Kolber, D.D., Michisaki, R.P., Foley, D.G., Chavez, F.P., 2009. Potential new production estimates in four eastern boundary upwelling ecosystems. *Prog. Oceanogr.* 83, 151–158.
- Messié, M., Chavez, F.P., 2015. Seasonal regulation of primary production in eastern boundary upwelling systems. *Prog. Oceanogr.* 134, 1–18.
- Montero, P., Daneri, G., Cuevas, L.A., González, H.E., Jacob, B., Lizárraga, L., Menchel, E., 2007. Productivity cycles in the coastal upwelling area off Concepción: the importance of diatoms and bacterioplankton in the organic carbon flux. *Prog. Oceanogr.* 75, 518–530.
- Montecino, V., Pizarro, G., Quiroz, D., 1996. Dinámica fitoplanctónica en el sistema de surgencia frente a Coquimbo (30°S) a través de la relación funcional entre fotosíntesis e irradiación (P-I). *Gayana Oceanológica* 4, 139–151.
- Nagai, T., Gruber, N., Frenzel, H., Lachkar, Z., McWilliams, J.C., Plattner, G.-K., 2015. Dominant role of eddies and filaments in the offshore transport of carbon and nutrients in the California Current System. *J. Geophys. Res.* 120, 5318–5341. <https://doi.org/10.1002/2015JC010889>.
- Nelson, D.M., Dortch, Q., 1996. Silicic acid depletion and silicon limitation in the plume of the Mississippi River: evidence from kinetic studies in spring and summer. *Mar. Ecol. Prog. Ser.* 136, 163–178.
- Pettitt, A.N., 1979. A non-parametric approach to the change-point problem. *J.R. Stat. Soc. Series C, Appl. Statistics* 28, 126–135.
- Plattner, G.K., Gruber, N., Frenzel, H., McWilliams, J.C., 2005. Decoupling marine export production from new production. *Geophys. Res. Lett.* 32. <https://doi.org/10.1029/2005GL022660>.
- Pino-Pinuer, P., Escribano, R., Hidalgo, P., Riquelme-Bugueño, R., Schneider, W., 2014. Copepod community response to variable upwelling conditions off central-southern Chile during 2002–2004 and 2010–2012. *Mar. Ecol. Prog. Ser.* 515, 83–95. <https://doi.org/10.3354/meps11001>.
- Pohlert, T., 2016. Non-parametric trend tests and change-point detection. Package ‘trend’. R package version 0.2.0, 26 pp.
- Quiñones, R.A., Gutiérrez, M.H., Daneri, G., Gutiérrez, D.A., González, H.E., Chávez, F., 2010. Pelagic carbon fluxes in the Humboldt Current System. In: Liu, K.K., Atkinson, L., Quiñones, R.A., Talaue-McManus, L. (Eds.), *Carbon and nutrient fluxes in global continental margins: A global synthesis*. Springer-Verlag, Berlin Heidelberg, IGBP Series Book, pp. 44–64.
- R Development Core Team, 2005. *R: A language and environment for statistical computing*. R Foundation for Statistical Computing, Vienna, Austria. ISBN 3-900051-07-0. <http://www.R-project.org>.
- Ragueneau, O., Tréguer, P., Leynaert, A., Anderson, R.F., Brzezinski, M.A., DeMaster, D.J., Dugdale, R.C., Dymond, J., Fischer, G., François, R., Heinze, C., Maier-Reimer, E., Martin-Jézéquel, V., Nelson, D.M., Quéguiner, B., 2000. A review of the Si cycle in the modern ocean: recent progress and missing gaps in the application of biogenic opal as a paleoproductivity proxy. *Global Planet. Change* 26, 317–365.
- Rivera, P., 1969. Sinopsis de las diatomeas de la bahía de Concepción. *Chile. Gayana Botánica* 18, 1–112.

- Rykaczewski, R.R., Checkley, D.M., 2008. Influence of ocean winds on the pelagic ecosystem in upwelling regions. *PNAS* 105, 1965–1970.
- Roemmich, D., McGowan, J., 1995. Climatic warming and the decline of zooplankton in the California Current. *Science* 267, 1324–1326.
- Sanchez, G.E., Lange, C.B., González, H.E., Vargas, G., Muñoz, P., Cisternas, C., Pantoja, S., 2012. Siliceous microorganisms in the upwelling center off Concepción, Chile (36S): Preservation in surface sediments and downcore fluctuations during the past ~150 years. *Progr. Oceanogr.* 92, 50–65.
- Santos, A.M.P., Kazmin, A.S., Peliz, A., 2005. Decadal changes in the Canary upwelling system as revealed by satellite observations: their impact on productivity. *J. Mar. Res.* 63, 359–379.
- Sarmiento, J.L., Simeon, J., Gnanadesikan, A., Gruber, N., Key, R.M., Schlitzer, R., 2007. Deep ocean biogeochemistry of silicic acid and nitrate. *Global Biogeochem. Cycles* 21, GB1S90.
- Shannon, C.E., Weaver, W., 1949. *The Mathematical Theory of Communication*. University of Illinois, Urbana, IL.
- Shannon, V., Crawford, R.J.M., Pollock, D.E., 1992. The 1980s – a decade of change in the Benguela ecosystem. In: Payne, A.L.L., Brink, K.H., Mann, K.H., Hilborn, R. (Eds.), *Benguela Trophic Functioning*. S. Afr. J. Marine Sci., pp. 271–296.
- Shapiro, S.S., Wilk, M.B., 1965. An analysis of variance test for normality. *Biometrika* 52, 591–599.
- Smith, S.V., Hollibaugh, J.T., 1997. Annual cycle and interannual variability of ecosystem metabolism in a temperate climate embayment. *Ecol. Monogr.* 67, 509–515.
- Sydeman, W.J., García-Reyes, M., Schoeman, D.S., Rykaczewski, R.R., Thompson, S.A., Black, B.A., Bograd, S.J., 2014. Climate change and wind intensification in coastal upwelling ecosystems. *Science* 345 (6192), 77–80. <https://doi.org/10.1126/science.1251635>.
- Smith, E.M., Kemp, W.M., 2001. Size structure and the production/respiration balance in a coastal plankton community. *Limnol. Oceanogr.* 46, 473–485.
- Snyder, M.A., Sloan, L.C., Dffenbaugh, N.S., Bell, J.L., 2003. Future climate change and upwelling in the California current. *Geophys. Res. Lett.* 30, 1823. <https://doi.org/10.1029/2003GL017647>.
- Schneider, W., Donoso, D., Garcés-Vargas, J., Escribano, R., 2017. Water-column cooling and sea surface salinity increase in the upwelling region off central Chile driven by a pole-ward displacement of the South Pacific High. *Oceanogr.* 151, 38–48.
- Sobarzo, M., Bravo, L., Donoso, D., Garcés-Vargas, J., Schneider, W., 2007. Coastal upwelling and seasonal cycles that influence the water column over the continental shelf off central Chile. *Progr. Oceanogr.* 75, 363–382.
- Strub, P.T., Mesías, J.M., Montecino, V., Rutllant, J., 1998. Coastal ocean circulation off western South America. In: Robinson, A.R., Brink, K.H. (Eds.), *The Global Coastal Ocean The Sea*. John Wiley & Sons, New York, NY, pp. 273–313.
- Strickland, J.D.H., 1960. Measuring the production of marine phytoplankton. *Bull. Fish. Res. Board Can.* 122, 1–72.
- Strickland, J.D.H., Parsons, T.R., 1972. *A practical handbook of seawater analysis*. *Bulletin of the Fisheries Research Board, Canada* 167, 310 pp.
- Teira, E., Serret, P., Fernández, E., 2001. Phytoplankton size-structure, particulate and dissolved organic carbon production and oxygen fluxes through microbial communities in the NW Iberian coastal transition zone. *Mar. Ecol. Progr. Ser.* 219, 65–83.
- Tomas, C.R., 1997. *Identifying Marine Phytoplankton*. Academic Press, pp. 858.
- Torres, R., Turner, D.R., Rutllant, J., Lefevre, N., 2003. Continued CO<sub>2</sub> outgassing in an upwelling area off northern Chile during the development phase of El Niño 1997–1998 (July 1997). *J. Geophys. Res.* 108 (C10), 3336. <https://doi.org/10.1029/2000JC000569>.
- Torres, R., Ampuero, P., 2009. Strong CO<sub>2</sub> outgassing from high nutrient low chlorophyll coastal waters off central Chile (30°S): The role of dissolved iron. *Estuar. Coast. Shelf. Sci.* 83, 126–132.
- Utermöhl, H., 1958. Vervollkommung der quantitativen Phytoplankton-Methodik. *Mitteilungen Internationale Vereinigung Theorie Angewandte Limnologie* 9, 1–38.
- Venrick, E.L., 1978. How many cells to count. In: Sounia, A. (Ed.), *Phytoplankton Manual*. *Monographs on Oceanographic Methodology* 6. UNESCO, pp. 167–180.
- Weeks, S.J., Currie, B., Bakun, A., Peard, K.R., 2004. Hydrogen sulphide eruptions in the Atlantic Ocean off southern Africa: implications of a new view based on SeaWiFS satellite imagery. *Deep-Sea Res.* 51, 153–172.
- Williams, P.J., Jenkinson, N.W., 1982. A transportable microprocessor controlled precise Winkler titration suitable for field station and shipboard use. *Limnol. Oceanogr.* 27, 576–584.
- Yamamoto, T., Tsuchiya, H., 1995. Physiological response of Si-limited *Skeletonema costatum* to silicate supply with salinity decrease. *Bull. Plankton Soc. Japan* 42, 1–17.
- Zentara, S.J., Kamykowski, D., 1981. Geographic variations in the relationship between silicic acid and nitrate in the South Pacific Ocean. *Deep Sea Res. Part A. Oceanographic Res. Papers* 28, 455–465.